

12-1-2020

Mobilization of iron stored in bacterioferritin is required for metabolic homeostasis in *Pseudomonas aeruginosa*

Achala N.D. Punchi Hewage
University of Kansas, Lawrence

Leo Fontenot
Louisiana State University

Jessie Guidry
LSU Health Sciences Center - New Orleans

Thomas Weldegiorghis
Louisiana State University

Anil K. Mehta
University of Florida

See next page for additional authors

Follow this and additional works at: https://digitalcommons.lsu.edu/chemistry_pubs

Recommended Citation

Punchi Hewage, A., Fontenot, L., Guidry, J., Weldegiorghis, T., Mehta, A., Donnarumma, F., & Rivera, M. (2020). Mobilization of iron stored in bacterioferritin is required for metabolic homeostasis in *Pseudomonas aeruginosa*. *Pathogens*, 9 (12), 1-26. <https://doi.org/10.3390/pathogens9120980>





This Article is brought to you for free and open access by the Department of Chemistry at LSU Digital Commons. It has been accepted for inclusion in Faculty Publications by an authorized administrator of LSU Digital Commons. For more information, please contact ir@lsu.edu.

Authors

Achala N.D. Punchi Hewage, Leo Fontenot, Jessie Guidry, Thomas Weldegiorghis, Anil K. Mehta, Fabrizio Donnarumma, and Mario Rivera

Article

Mobilization of Iron Stored in Bacterioferritin Is Required for Metabolic Homeostasis in *Pseudomonas aeruginosa*

Achala N. D. Punchi Hewage ¹, Leo Fontenot ², Jessie Guidry ³, Thomas Weldeghiorghis ², Anil K. Mehta ⁴, Fabrizio Donnarumma ² and Mario Rivera ^{2,*}

¹ Department of Chemistry, University of Kansas, 2030 Becker Dr., Lawrence, KS 66047, USA; achala@ku.edu

² Department of Chemistry, Louisiana State University, 232 Choppin Hall, Baton Rouge, LA 70803, USA; lfont39@lsu.edu (L.F.); thomaskw@lsu.edu (T.W.); fabrizio@lsu.edu (F.D.)

³ Department of Biochemistry and Molecular Biology, Louisiana State University Health Science Center, 1901 Perdido Street, New Orleans, LA 70112, USA; jjguid@lsuhsc.edu

⁴ National High Magnetic Field Laboratory, University of Florida, 1149 Newell Drive, Gainesville, FL 32610, USA; anil.mehta@ufl.edu

* Correspondence: mrivera@lsu.edu

Received: 16 October 2020; Accepted: 23 November 2020; Published: 24 November 2020



Abstract: Iron homeostasis offers a significant bacterial vulnerability because pathogens obtain essential iron from their mammalian hosts, but host-defenses maintain vanishingly low levels of free iron. Although pathogens have evolved mechanisms to procure host-iron, these depend on well-regulated iron homeostasis. To disrupt iron homeostasis, our work has targeted iron mobilization from the iron storage protein bacterioferritin (BfrB) by blocking a required interaction with its cognate ferredoxin partner (Bfd). The blockade of the BfrB–Bfd complex by deletion of the *bfd* gene (Δbfd) causes iron to irreversibly accumulate in BfrB. In this study we used mass spectrometry and NMR spectroscopy to compare the proteomic response and the levels of key intracellular metabolites between wild type (wt) and isogenic Δbfd *P. aeruginosa* strains. We find that the irreversible accumulation of unusable iron in BfrB leads to acute intracellular iron limitation, even if the culture media is iron-sufficient. Importantly, the iron limitation and concomitant iron metabolism dysregulation trigger a cascade of events that lead to broader metabolic homeostasis disruption, which includes sulfur limitation, phenazine-mediated oxidative stress, suboptimal amino acid synthesis and altered carbon metabolism.

Keywords: iron homeostasis; iron metabolism; sulfur metabolism; *Pseudomonas aeruginosa*; ferritin; bacterioferritin; ferredoxin; proteomics

1. Introduction

Pseudomonas aeruginosa is an opportunistic pathogen causative of severe infections, particularly in health care settings and in immunocompromised patients. The emergence and dissemination of multidrug-resistant *Pseudomonas aeruginosa* strains is a significant threat to public health [1–3]. The World Health Organization included carbapenem-resistant *P. aeruginosa* in its priority list of pathogens for which new antibiotics are urgently needed [4]. To combat the threat posed by multidrug-resistant organisms, there is an urgent need to discover novel antibiotics and validate new targets in antibacterial research [5–7]. A new approach to combat infection currently under investigation is to capitalize on the iron requirement of pathogens for establishing infections [8–14]. Iron is essential because of its requirements of enzymes mediating respiration, DNA synthesis, amino acid synthesis and many other key metabolic processes [15]. Pathogens must obtain iron from their host, but host nutritional immunity

denies the essential nutrient by maintaining very low concentrations of free iron ($\sim 10^{-20}$ M) [15]. The chemical properties of iron also present challenges to invading pathogens in that the reactivity of the ferrous ion (Fe^{2+}) toward H_2O_2 and O_2 induces oxidative stress. Consequently, bacterial iron homeostasis (iron acquisition, storage and utilization) is highly regulated to ensure sufficiency for metabolic needs while preventing iron-induced toxicity [16,17].

The struggle for iron between host and bacteria has given rise to the idea of exploiting iron metabolism as a potentially viable approach to develop new antibiotics. Approaches that follow this general idea include the development of siderophore conjugates to enhance antibiotic cell penetration [18,19], the sequestration of iron with chelators to deplete intra- and extracellular iron [13,20–23], the perturbation of heme uptake or heme degradation to deny the pathogens a rich iron source during infections [12,24], and the utilization of Ga^{3+} , which is aimed at systemically replacing Fe^{3+} with Ga^{3+} in the active site of enzymes [25,26]. Dysregulation of iron metabolism is also thought to offer a significant vulnerability. To disrupt iron metabolism, our laboratories are studying a new and specific target in *Pseudomonas aeruginosa*, a protein–protein interaction between the iron storage protein bacterioferritin (BfrB) and its physiological partner, the bacterioferritin-associated ferredoxin (Bfd) [27]. Our work has demonstrated that although two ferritin-like proteins (FtnA and BfrB) coexist in *P. aeruginosa* [28], BfrB is the main iron storage protein [16]. BfrB is a spherical molecule assembled from 24 subunits which contains an interior cavity ~ 80 Å in diameter where up to ~ 3000 Fe^{3+} ions can be stored (Figure 1A). The BfrB structure also harbors heme molecules sandwiched between two subunits, buried under the external protein surface [27,29]. The mobilization of iron stored in BfrB requires Bfd. The X-ray crystal structure of the BfrB–Bfd complex revealed that up to 12 Bfd molecules can bind at identical sites on the BfrB surface, between two subunits, and immediately above a heme molecule. The function of the heme is to facilitate electron transfer from the [2Fe-2S] cluster in Bfd to the Fe^{3+} stored in the interior cavity, thus facilitating the release of Fe^{2+} to the cytosol (Figure 1B) [30].

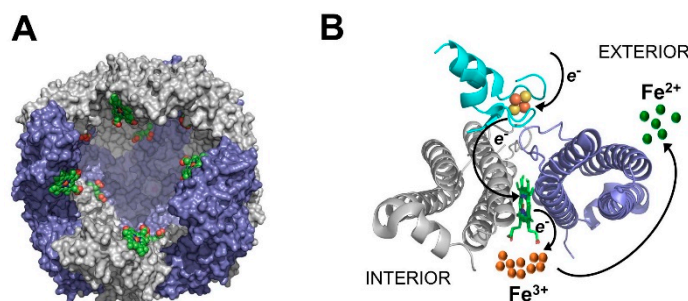


Figure 1. (A) Bacterioferritin (BfrB) from *Pseudomonas aeruginosa* (PDB ID 3is7) is a spherical and hollow protein capable of storing up to 3000 Fe^{3+} ions in its interior cavity. Heme molecules (green) are buried under the protein exterior, bound between each two subunits, with the heme propionates exposed to the interior cavity. (B) Structure of the BfrB–Bfd complex (PDB ID 4e6k) depicting Bfd (cyan) binding between two BfrB subunits (grey and blue), immediately above a heme molecule. Electron transfer from the [2Fe-2S] cluster in Bfd to the Fe^{3+} in the BfrB interior, which is facilitated by the heme, enables mobilization of Fe^{2+} to the cytosol.

Studies conducted with a *P. aeruginosa* strain where the *bfd* gene has been deleted (Δbfd), demonstrated that blocking the BfrB–Bfd complex causes the irreversible accumulation of iron in BfrB and low levels of free iron in the cytosol [16]. The same study showed that culturing planktonic Δbfd cells in low iron media results in lower cell density than similar cultures of the wild type (wt) strain. In contrast, when cultured in iron-sufficient media (10 μM), the wt and Δbfd cells grow at the same rate and to the same cell density. In the stationary phase, however, the Δbfd cells secrete several-fold more pyoverdine (an Fe^{3+} siderophore) than the wt cells, suggesting that the blockade of the BfrB–Bfd complex induces iron limitation in the *P. aeruginosa* cells [16]. Additional investigations showed that the Δbfd cells form poorly developed biofilms, even in iron-sufficient conditions, and that the biofilm-embedded cells

exhibit cytosolic iron deficiency [14]. Given that *P. aeruginosa* cells require sufficient intracellular iron to establish mature biofilms [31], it was suggested that the irreversible accumulation of iron in BfrB in the Δbfd cells causes iron limitation, even in iron-sufficient conditions [14]. Similarly, challenging planktonic cells with small molecule inhibitors of the BfrB–Bfd complex causes nearly irreversible accumulation of iron in BfrB, a growth phenotype and pyoverdine hyper production [10].

Although these observations were interpreted to suggest that the blockade of the BfrB–Bfd complex may result in iron metabolism dysregulation that adversely affects *P. aeruginosa* fitness, the connections between iron metabolism dysregulation and cellular metabolic homeostasis are not yet known [10]. To begin understanding these connections, we interrogated the global cellular response to blocking the BfrB–Bfd complex in *P. aeruginosa* by comparing the proteomic profiles of wt and Δbfd cells cultured in iron-sufficient media. We found that blocking the BfrB–Bfd complex indeed leads to iron metabolism dysregulation and systemic iron limitation. The lesion in iron metabolism triggers a cascade of events, leading to phenazine overproduction and associated redox stress, which impose iron and sulfur limitation, altered carbon metabolism and suboptimal amino acid biosynthesis.

2. Results and Discussion

Deletion of the *bfd* gene results in the irreversible accumulation of iron in BfrB and concomitant low iron levels in the cytosol [16]. These observations, however, did not indicate whether the low iron levels are confined to the free iron pool in the cytosol, or if iron limitation also affects iron-dependent proteins and the processes in which these proteins participate. Answering this question requires that the experimental approach enable a relatively global assessment of the bacterial cell response to blocking the BfrB–Bfd complex. Consequently, we compared the proteomic profiles of the wild type (wt) *P. aeruginosa* PAO1 and the isogenic Δbfd mutant cultured under identical conditions. As indicated above, both strains grow at the same rate and to a nearly identical cell density when cultured in iron-sufficient media. During the stationary growth phase, however, the Δbfd cells secrete several-fold more pyoverdine than the wt cells because of relatively low cytosolic iron levels [16]. Consequently, we harvested the cells 30 h post inoculation when the Δbfd cells secreted approximately sixfold more pyoverdine than their wt counterparts (Figure S1). To compare the proteomic profiles of the wt and Δbfd mutant cells, we carried out Tandem Mass Tag (TMT) labeling, an isobaric covalent modification of primary amines which enables relative quantification of proteins across multiple samples [32], upstream of the mass spectrometric analysis. This approach allowed us to identify and quantitate 3210 proteins, approximately 54% of the total 5570 proteins in *P. aeruginosa* [33]. Three biological replicates and experimental (three each) replicates were incorporated so that *t*-tests were performed on the 3210 proteins to determine significant differences in protein abundance between wt and Δbfd cells ($p < 0.05$). Proteins exhibiting a Δbfd /wt fold change (FC) ≥ 1.4 (\log_2 FC ≥ 0.5) are considered enriched in the Δbfd cells, and proteins with a Δbfd /wt FC ≤ 0.7 (\log_2 FC ≤ -0.5) are considered depleted [34]. The results are summarized in a volcano plot (Figure 2) where the segmented vertical lines indicate \log_2 FC ± 0.5 and the horizontal segmented line denotes $p = 0.05$. Of the 3210 identified proteins, 296 (~9%) are above or below the cutoff, 159 are enriched (128 $p < 0.05$) and 137 are depleted (96 $p < 0.05$) in Δbfd relative to wt cells.

The differentially expressed proteins were functionally categorized using the Kyoto Encyclopedia of Genes and Genomes (KEGG) Orthology classification [35] (Figure 2B), the *Pseudomonas* Genome Database [36], and the UniProt database [37]. This analysis revealed that the inhibition of the BfrB–Bfd complex causes significant changes in the proteins involved in iron metabolism (Table S1). The significant enrichment of proteins involved in iron and heme acquisition in the Δbfd relative to the wt cells is consistent with a strong iron starvation response caused by the irreversible accumulation of iron in BfrB when the BfrB–Bfd complex is inhibited [16]. Accordingly, proteins involved in the biosynthesis of 4-hydroxy-2-alkylquinolines (HAQs) and phenazines are also enriched in the Δbfd cells. Importantly, the data also reveal strong connections between the iron starvation response and carbon metabolism, sulfur metabolism, amino acid biosynthesis, respiration, oxidative stress defense,

and cellular transport (Table S1). These findings also indicate that the blockade of the BfrB–Bfd complex is a new approach to establishing intracellular iron starvation without treating the culture media with iron chelators, which can deplete it of other metal ions.

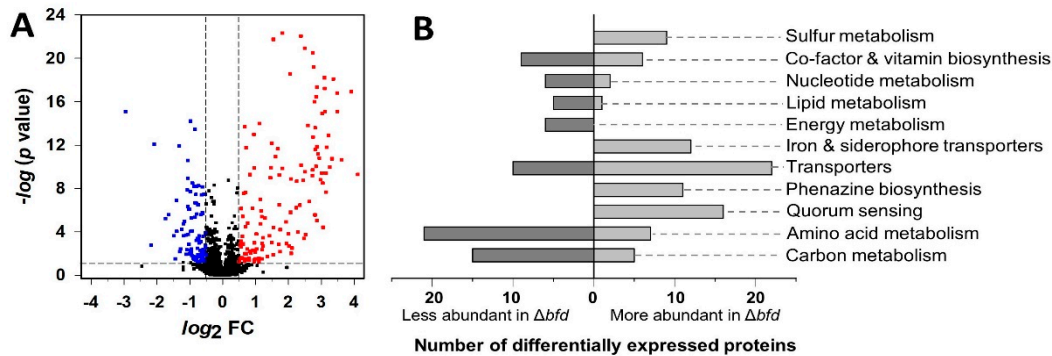


Figure 2. (A) Volcano plot illustrating differentially abundant proteins in the Δbfd isogenic mutant relative to the wt strain. The fold change (FC) is defined as the abundance ratio of Δbfd /wt. The non-axial vertical lines designate $\log_2 FC \pm 0.5$ and the non-axial horizontal line denotes $p = 0.05$. Points in red represent proteins more abundant in the Δbfd mutant, while points in blue indicate proteins less abundant in the mutant. (B) KEGG Orthology functional classification of proteins differentially expressed in wt and Δbfd cells.

2.1. Inhibition of Iron Mobilization from BfrB Elicits a Global Iron Starvation Response

2.1.1. Pyoverdine Biosynthesis

The Δbfd cells overproduce pyoverdine (Figure S1), a siderophore secreted by *P. aeruginosa* to assimilate iron [38]. Pyoverdine molecules are composed of three main parts, a dihydroquinoline chromophore (fluorescent), a strain-specific peptide, and a side chain stemming from the chromophore. *P. aeruginosa* produces three pyoverdines (PVDI–III), each characterized by a different peptide chain [39]; PVDI (PVD hereafter) is the best characterized. PVD biosynthesis, schematically summarized in Figure 3, requires numerous enzymes and non-ribosomal peptide synthetases (NRPSs) [38,40,41]. Inspection of Figure 3 shows that all the enzymes and non-ribosomal peptides involved in the biosynthesis, secretion and import of the iron–PVD complex are strongly enriched in the Δbfd cells, as indicated by the color scale. The PVD backbone begins assembly in the cytosol with the aid of NRPSs, PvdA, PvdD, PvdF, PvdH, PvdI, PvdJ and PvdL. The cytoplasmic (non-fluorescent) PVD precursor bound to a myristic or myristoleic acid chain [42] is thought to be transported into the periplasm by the ABC transporter PvdE [43], which is also highly enriched in the Δbfd cells. The maturation of PVD occurs in the periplasm where PvdQ cleaves the myristic or myristoleic moiety to produce ferriabactin, which is matured by enzymes PvdN, PvdM, PvdO, and PvdP, all significantly enriched in the Δbfd cells. The siderophore is secreted through a tripartite efflux pump consisting of an inner membrane protein (PvdT), periplasmic adaptor protein (PvdR) and outer membrane protein (OpmQ) [41,44,45]. The secreted PVD chelates Fe^{3+} and the complex is taken into the periplasm by FpvA in a TonB-dependent manner [46,47], where it binds to periplasmic proteins FpvC and FpvF. The cytoplasmic membrane protein FpvG is thought to reduce the chelated Fe^{3+} , probably aided by proteins FpvH, FpvJ, and FpvK [48]. After its dissociation from PVD, Fe^{2+} binds to FpvC and is transported to the cytoplasm by the ABC transporter FpvDE, and PVD is recycled into the extracellular space via the PvdT–PvdR–OpmQ efflux pump. We also observe that the sigma factor PvdS, required for the expression of pyoverdine, is enriched in the Δbfd cells, whereas the anti-sigma factor FpvR, which is required to inactivate PvdS, is strongly attenuated. As such, the proteomic profiles are in excellent agreement with the pyoverdine overproduction of the Δbfd relative to the wt cells.

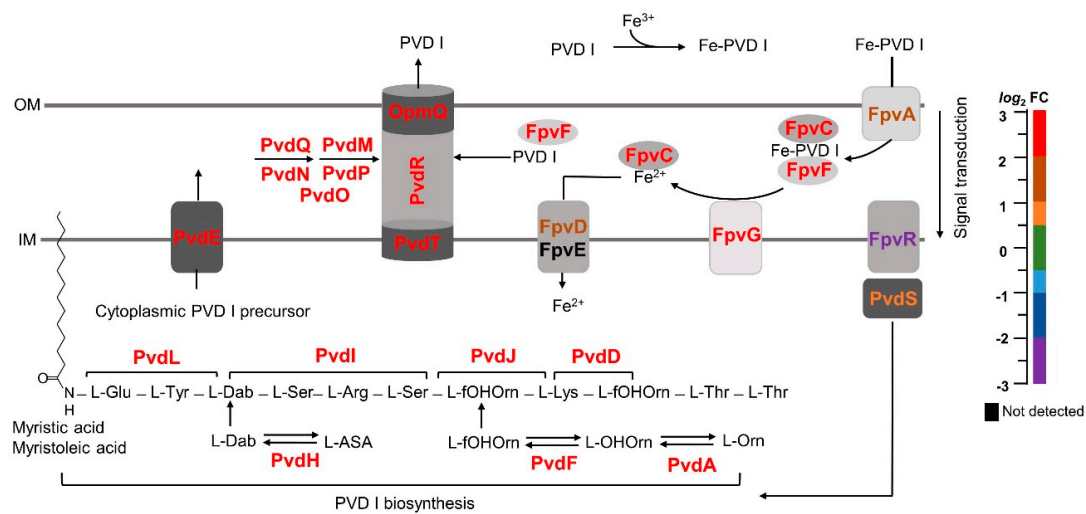


Figure 3. Proteins for pyoverdine (PVD I) assembly and function are enriched in the $\Delta b f d$ mutant. The schematic shows PVD I assembly, which is initiated in the cytosol, and matured in the periplasm prior to its secretion to the extracellular milieu. Extracellular PVD I binds Fe³⁺, the Fe³⁺-PVD I complex is internalized to the periplasm where a reductase system facilitates the release of Fe²⁺ and PVD I; the former is transported to the cytosol and the PVD I is recirculated to the extracellular space. The relative abundance ($\Delta b f d$ /wt) of each of the proteins involved in these processes is color coded according to the log₂FC scale. Outer membrane (OM), inner membrane (IM).

2.1.2. Pyochelin Biosynthesis

Pyochelin (PCH) is a lower affinity siderophore relative to pyoverdine, which at neutral pH chelates Fe³⁺ with 2:1 stoichiometry. The biosynthesis of pyochelin involves three NRPS and far fewer proteins than the biosynthesis of pyoverdine. It is schematically depicted in Figure 4A where the relative abundance of proteins in the $\Delta b f d$ relative to the wt cells is indicated by the color scale. Pyochelin biosynthesis starts with the transformation of chorismate to salicylate by enzymes PchA and PchB [49,50], both enriched in the $\Delta b f d$ cells. Salicylate is then activated and coupled to a molecule of activated L-cysteine with the aid of enzymes PchD, PchC and PchE to produce hydroxyphenyl-thiazoline [51,52]; PchF catalyzes the incorporation of a second molecule of activated L-cysteine to form the second thiazoline ring, which is reduced to thiazolidine by PchG, before PchF catalyzes the release of pyochelin [53]. The synthesis of PCH takes place in the cytosol, but not much is yet known regarding the proteins involved in its secretion, or the import of iron-bound PCH. In this context, Figure 4B shows the organization of genes involved in pyochelin biosynthesis and function [50], colored with the relative abundance of the corresponding proteins in the proteomics data set. This representation demonstrates that all the proteins involved in pyochelin biosynthesis and function are enriched in the $\Delta b f d$ cells.

2.1.3. Heme Uptake

P. aeruginosa utilizes two systems to scavenge host-heme, a hemophore-dependent heme assimilation system (*has*) and a non-hemophore-dependent *Pseudomonas* heme uptake (*phu*) system [54,55]. Heme is extracted from hemoglobin by the TonB-dependent PhuR receptor for transport across the outer membrane. In the periplasmic space heme is shuttled by PhuT to the PhuUVW transporter for internalization into the cytosol, where it is sequestered by PhuS and transferred to the heme oxygenase (HemO) [56], which cleaves the heme macrocycle to release iron, biliverdin- β , biliverdin- δ and carbon monoxide [57]. Consistent with the iron starvation caused by the blockade of the BfrB-Bfd complex, most of the enzymes involved in heme capture, internalization and heme degradation are enriched in the $\Delta b f d$ cells (Figure 5).

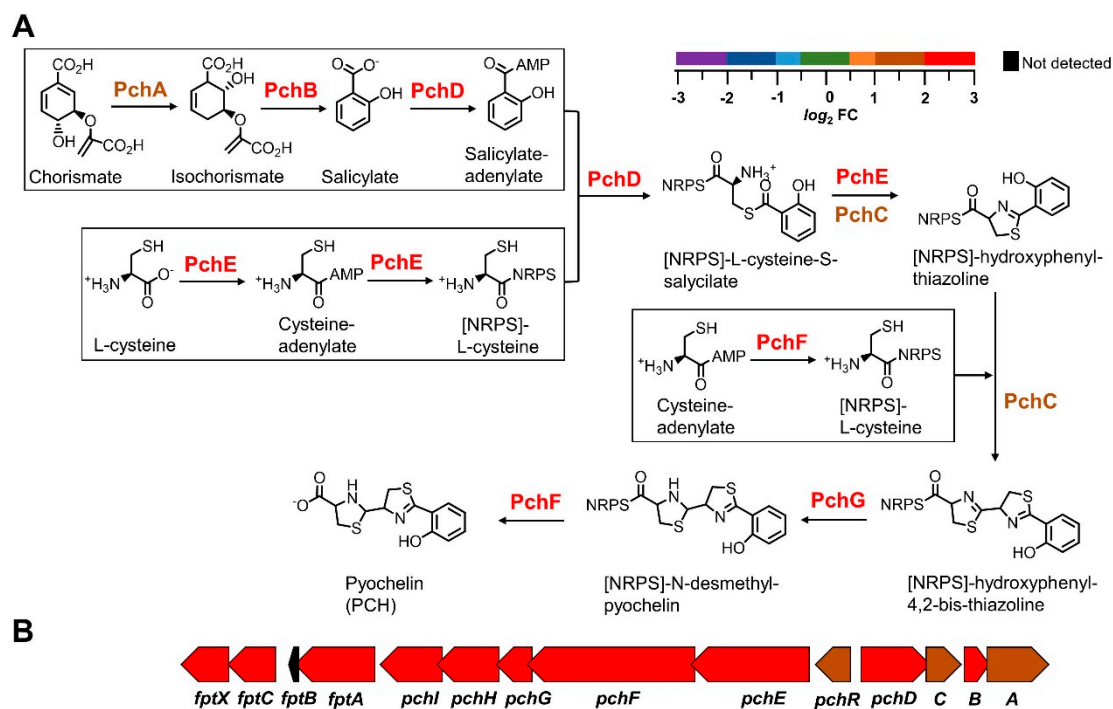


Figure 4. Proteins for the synthesis and function of pyochelin are enriched in the Δbld cells. (A) Schematic depiction of pyochelin (PCH) biosynthesis, which starts with chorismate and requires two equivalents of L-cysteine. The relative abundance ($\Delta bld/wt$) of each of the proteins involved in PCH biosynthesis is color coded according to the \log_2FC scale. (B) Organization of the genes encoding proteins for PCH biosynthesis and function color coded according to the \log_2FC scale.

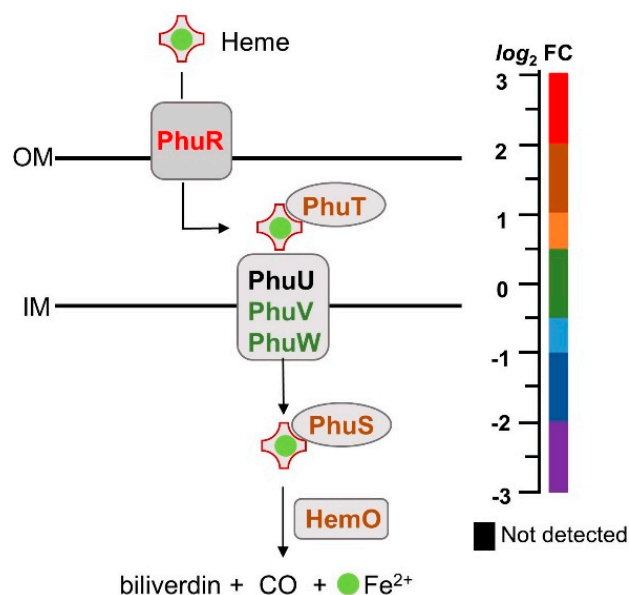


Figure 5. Proteins for heme capture, internalization and release of heme-iron are enriched in the Δbld cells. The relative abundance ($\Delta bld/wt$) of the proteins involved in these processes is indicated by the color according to the \log_2FC scale. Outer membrane (OM), inner membrane (IM).

2.1.4. *Pseudomonas* Quinolone Signal

The conditions of iron starvation are known to stimulate the biosynthesis of 2-alkyl-4-quinolones (AQs), such as HHQ (2-heptyl-4-hydroxyquinolone), PQS (2-heptyl-3-hydroxy-4-quinolone) and HQNO (2-heptyl-4-hydroxyquinoline-N-oxide). The *pqs* system (Figure 6A) encompasses the *pqsR* gene, the *pqsABCDE-phnAB* operon and the distally located *pqsH* and *pqsL* genes [58]. The enzymes coded by the *pqs* system synthesize HHQ and PQS, which stimulate the expression of the *pqs* operon [59]. Low iron conditions stimulate the biosynthesis of AQs by at least two mechanisms: (i) the iron starvation σ factor PvdS increases transcription of *pqsR* via an iron starvation box [60,61], and (ii) the PrrF sRNAs (PrrF1 and PrrF2), which are expressed under low iron conditions, repress the transcription of genes coding for enzymes that catalyze the degradation of anthranilate (*antABC* and *catBCA*), therefore sparing anthranilate for the biosynthesis of AQs [62,63]. The biosynthetic process, schematically shown in Figure 6B, starts when PqsA converts anthranilate into anthraniloyl-CoA, which is converted to 2-aminobenzoylacetyl-CoA (2-ABA-CoA) by PqsD and then to 2-aminobenzoylacetate (2-ABA) by PqsE. The condensation of 2-ABA with octanoyl-CoA, catalyzed by the PqsBC heterodimer, forms HHQ. Under aerobic conditions HHQ is oxidized to PQS by the enzyme PqsH, whereas the biosynthesis of HQNO, which is also produced from 2-ABA, requires the monooxygenase PqsL and the PqsBC heterodimer [64,65].

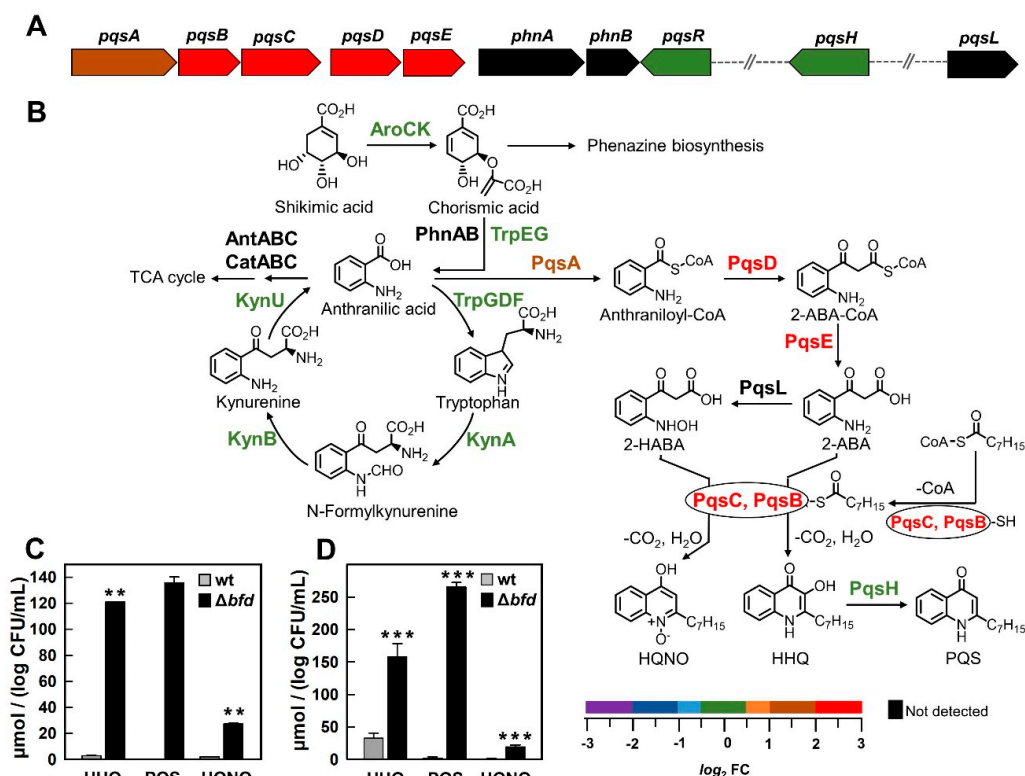


Figure 6. Proteins for the synthesis of AQs are enriched in the Δbdf cells. (A) Organization of the genes encoding proteins for AQ biosynthesis, and the *phnAB* genes, color coded according to the \log_2FC scale. (B) Schematic representation of the biosynthesis of AQs showing the relative abundances ($\Delta bdf/wt$) of each of the proteins in the pathway color coded according to the \log_2FC scale. The preparation of this scheme was aided significantly by ref [64]. (C,D) LC-MS-determined levels of HHQ, PQS, and HQNO from cells and from spent media, respectively, obtained from cultures of wt and Δbdf cells; PQS from wt cells was below the detection limit. The amount of AQs has been normalized to $\log CFU/mL$. Means and standard deviations from three biological replicates are shown. 2-aminobenzoylacetyl-CoA (2-ABA-CoA), 2-aminobenzoylacetate (2-ABA), 2-hydroxylaminobenzoylacetate (2-HABA). $p < 0.01$ denoted by ** and $p < 0.001$ by *** relative to wt.

All the enzymes involved in the conversion of anthranilate to HHQ (*pqsABCDE*) are enriched in the Δbfd cells. In contrast, the enzyme required to convert 2-ABA to 2-HABA (PqsL) was not detected, and the enzyme required to convert HHQ to PQS (PqsH) is expressed in the Δbfd cells at the same levels as in the wt cells (Figure 6B). In order to understand how this pattern of relative protein expression is manifested in the levels of AQs produced by the wt and Δbfd cells, we used liquid chromatography-mass spectrometry (LC-MS) to quantitate HHQ, PQS and HQNO in the cells and in the cell-free supernatants. These values, normalized to CFU/mL to enable comparisons (Figure 6C,D), demonstrate that the Δbfd cells produce significantly higher levels of AQs than the wt cells, observations that agree with the enrichment of enzymes encoded by the *pqsABCDE* genes in the mutant. It is also interesting to consider that HHQ and PQS are produced and secreted by the Δbfd cells at relatively similar levels, despite the observation that PqsH is not enriched in Δbfd relative to wt. This is probably because the abundance of HHQ in the Δbfd cells stimulates the activity of PqsH, thus producing relatively high levels of PQS, even if the enzyme is not enriched relative to the wt cells. Along the same vein, the abundance of HHQ in the Δbfd cells probably stimulates the activity of PqsL (not detected) by channeling a fraction of 2-ABA toward 2-HABA, which is converted to HQNO by the PqsBC heterodimer. It is tempting to speculate that the relatively low levels of HQNO relative to HHQ and PQS suggest that the synthesis of HQNO is throttled down, possibly by maintaining low levels of the PqsL enzyme.

Anthranilate, the first committed precursor in the biosynthesis of AQs, can be synthesized from shikimate by AroCK and the anthranilate synthases PhnAB and TrpEG, or via the kynurenine pathway that converts tryptophan into anthranilate [66] (see Figure 6B). We observed no changes in the levels of enzymes involved in the kynurenine pathway or in the enzymes that convert shikimate to anthranilate between wt and Δbfd cells. This is most likely because the peptone in PI media is a rich source of tryptophan, which can be used for anthranilate biosynthesis.

Iron limiting conditions are thought to spare anthranilate for the biosynthesis of AQs by downregulating AntABC and CatABC, the enzymes implicated in the first steps of anthranilate degradation for its incorporation in the TCA cycle [62]. We did not detect AntABC and CatABC in our experiments; nevertheless, the enrichment of enzymes involved in the biosynthesis of AQs, the higher levels of AQs found in the Δbfd cells, and the “normal” production of anthranilate in the Δbfd cells, corroborate that when experiencing iron limitation, *P. aeruginosa* cells indeed utilize anthranilate resources for the biosynthesis of AQs.

2.1.5. Phenazines

Although *P. aeruginosa* can produce up to five different phenazine derivatives [67,68], pyocyanin (PYO) is the most studied phenazine in this organism. Phenazine biosynthesis is carried out by enzymes produced from the transcription of two similar operons, *phzA1B1C1D1E1F1G1* (*phz1*) and *phzA2B2C2D2E2F2G2* (*phz2*) [67]. HHQ and PQS are known to positively regulate the expression of *phz1* and *phz2* [69], and recent studies have shown that the enzyme PqsE also stimulates transcription of the *phz1* and *phz2* operons [65]. As such, iron limitation, which stimulates the *pqsABCDE-phnAB* operon (see above), is also expected to stimulate transcription of the *phz* operons via HHQ, PQS and PqsE, all of which are enriched in the Δbfd cells (see Figure 6). In agreement with this idea, the data presented in Figure 7 show that several of the enzymes encoded by genes in the *phz1* and *phz2* operons are enriched in the Δbfd cells relative to wt. The enrichment of enzymes coded by both operons is also in agreement with a previous report demonstrating that enzymes from the *phz1* and *phz2* operons participate in the biosynthesis of phenazine-1-carboxylic acid (PCA) in planktonic cells [70]. Inspection of Figure 7B shows that in the path converting chorismic acid to PCA, at least one of the required enzymes from the *phz1* or *phz2* operons is enriched in the Δbfd cells. In comparison, the enzymes required for the conversion of PCA to 5MPCA (PhzM) and then to PYO (PhzS) exhibit the same levels as in the wt cells. To understand the consequences of this enrichment pattern on the production of phenazines, we analyzed the total levels of PCA and PYO; 5MPCA was not analyzed due to being unstable [71].

The results (Figure 7C) show that the Δbfd cells produce approximately threefold more PCA and PYO than the wt cells, observations that are in excellent agreement with the enrichment of the enzymes required to convert chorismic acid to PCA. The enhanced production of PYO by the Δbfd cells with “normal” levels of PhzS is probably due to its stimulation by the abundance of PCA. The potential consequences of PCA overproduction in the Δbfd cells are important and will be discussed below.

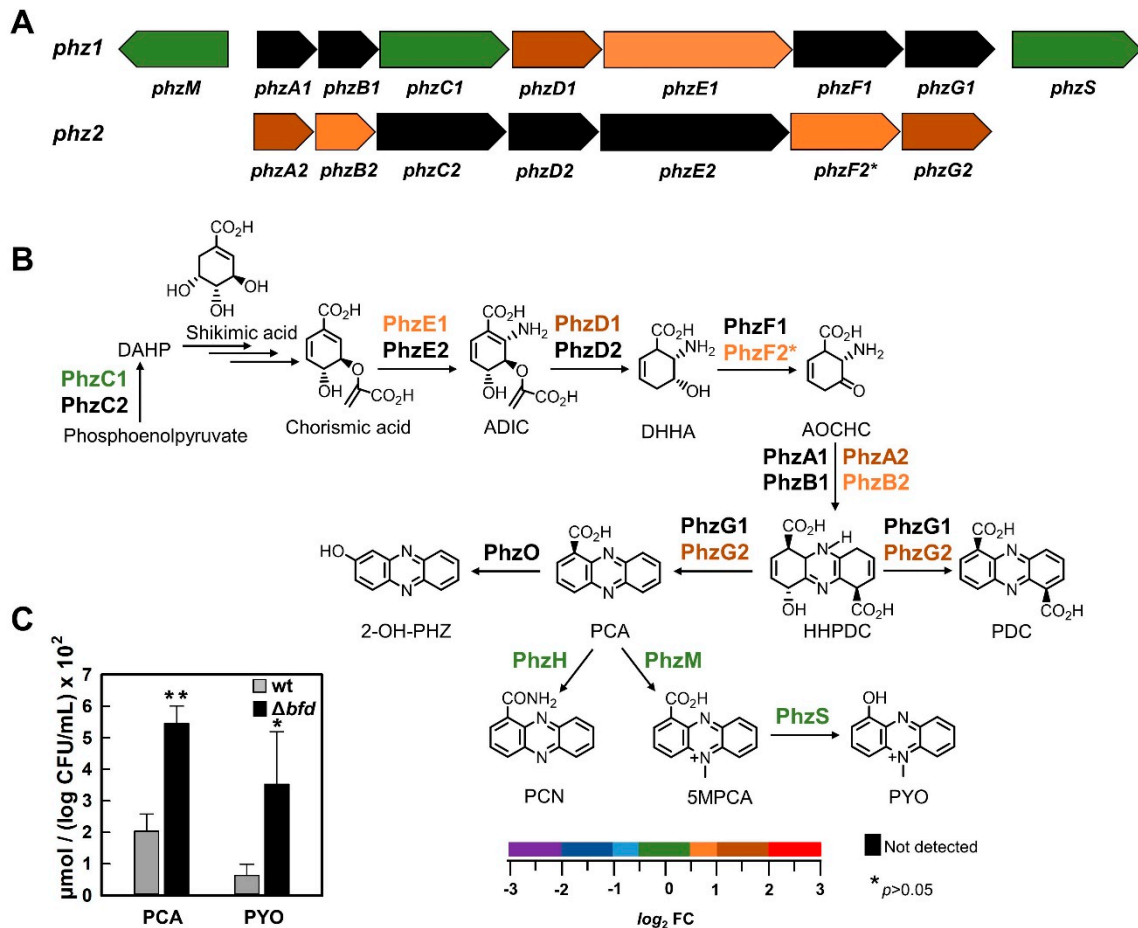


Figure 7. Proteins for the biosynthesis of phenazines are enriched in the Δbfd cells. (A) Organization of the genes in the two operons, *phz1* and *phz2*, color coded according to the \log_2FC scale. (B) Schematic representation for the biosynthesis of phenazines showing the relative abundances ($\Delta bfd/wt$) of each of the proteins in the pathway color coded according to the \log_2FC scale. The preparation of this scheme was aided significantly by ref. [68]. (C) LC-MS-determined levels of PCA in wt and Δbfd cells normalized to $\log CFU/mL$. 2-amino-2-desoxyisochorismic acid (ADIC), *trans*-2,3-dihydro-3-hydroxyanthranilic acid (DHHA), 6-amino-5-oxocyclohex-2-ene-1-carboxylic acid (AOCHC), hexahydrophenazine-1,6-dicarboxylic acid (HHPDC), phenazine-1-carboxylic acid (PCA), 5-methyl-phenazine-1-carboxylic acid (5MPCA), phenazine-1-carboxamide (PCN), pyocyanin (PYO), 2-hydroxy-phenazine (2-OHPHZ). $p < 0.05$ denoted by * and $p < 0.01$ by ** relative to wt.

2.2. Inhibition of Iron Mobilization from BfrB Affects Central Carbon Metabolism and Amino Acid Biosynthesis

Comparing the proteomic profiles of wt and Δbfd cells shows significant differences in central carbon metabolism, which extend to the synthesis of several amino acids (Figure 8). We begin this discussion by pointing to the enrichment of enzymes involved in the conversion of glycogen to glucose (PA2152 and TreA) [72–74] in the Δbfd cells. Glycogen is a major intracellular reserve polymer of the α -1-4-linked glucose monomers that accumulates in bacterial cells under conditions of limited growth, and it is degraded when carbon is limited [75–79]. As such, the enrichment of PA2152 and TreA in the

Δbfd cells suggests alterations in carbon metabolism. Previous studies comparing the metabolic flux of exponential phase *Pseudomonas putida* cells grown in iron replete vs. iron limiting conditions showed a decrease in metabolic flux through the Entner–Doudoroff route, as well as through Fe-containing metabolic enzymes of the tricarboxylic acid (TCA) cycle [80]. In agreement, our results show that several enzymes of the cycle are depleted in the Δbfd cells (Figure 8). Enzymes in the upper portion of the TCA cycle which catalyze the conversion of pyruvate (AcoC, PA3417) or butanediol (AcoA, AcoB, AcoC) to acetyl-CoA [81] are depleted in the Δbfd cells. In addition, the aconitase enzymes AcnA and PA0794, which depend on [4Fe-4S] catalytic centers to transform citrate to isocitrate via cis-aconitate, are also depleted in the mutant cells. In the bottom section of the TCA cycle, the conversion of fumarate to malate is probably affected by the depletion of FumA (an iron-dependent enzyme). The depletion of FumA in the mutant cells appears to be compensated by the significant enrichment of FumC1, an iron-independent fumarase hydratase, whose expression is known to be stimulated under iron limiting conditions [82].

The iron starvation caused by blocking the BfrB–Bfd complex also affects amino acid biosynthesis. Glycine plays an essential role as a precursor of proteins, nucleic acids and other metabolites. Glycine can be produced from choline via glycine-betaine (GB) and sarcosine, or from serine, as schematically depicted in Figure 8. *P. aeruginosa* can use GB as a sole source of carbon, nitrogen, and energy through a series of successive demethylation reactions that produce Gly [83,84]. Although the reasons are not yet clear, *P. aeruginosa* maintains intracellular pools of GB, the sizes of which are affected by the main carbon source, temperature or salinity [85]. Our results indicate that the GB pool is affected by iron limitation because both proteins required to convert GB to dimethylglycine (GbcA and GbcB) are iron-dependent; GbcA is significantly depleted in the Δbfd cells and GbcB was not detected. The demethylation of dimethylglycine is catalyzed by DgcA and DgcB, and the product of the reaction, sarcosine, is known to stimulate the sarcosine oxidation and utilization regulator (SouR), thereby inducing the *soxBDA* operon, along with a serine hydroxymethyl transferase (GlyA1) [86]. The SoxBDA enzymes catalyze the conversion of sarcosine to glycine, while GlyA1 catalyzes the catabolism of glycine to serine. Consistent with the depletion of DgcA and probable relatively low conversion of dimethylglycine to sarcosine in the mutant cells, the SoxBDA and GlyA1 enzymes are also depleted (Figure 8), suggesting that the assimilation of GB and sarcosine to Gly and Ser is adversely affected by the blockade of the BfrB–Bfd complex. As such, iron limitation in the Δbfd cells adversely affects the pathways that transform GB and sarcosine into metabolites used for energy production and biosynthesis. It is probable that the sensitivity of this path to iron depletion starts with a fraction of the iron-dependent enzymes unable to assemble functional catalytic centers, initially affecting sarcosine biosynthesis, which in turn represses transcription of the SoxBDA and GlyA1 enzymes and affects the biosynthesis of Gly and Ser.

The iron starvation elicited by blocking the BfrB–Bfd complex appears to also affect the biosynthesis of several other amino acids whose structures are formed from intermediates in the TCA cycle. Ala, Leu, Ile and Val are derived from pyruvate. The biosynthesis of Leu and Ile requires the large and small subunits of the iron-dependent 3-isopropylmalate dehydratase (LeuC and LeuD) and PA3506, which are depleted in the Δbfd cells (Figure 8). The synthesis of Glu, Gln and Lys may also be impacted by depletion of the iron-dependent aconitase enzymes AcnA and PA0794, required to transform citrate to isocitrate. We used NMR spectroscopy (see Materials and Methods) to identify and measure the relative concentrations of several of these amino acids in the wt and Δbfd cells. The results from these experiments (Figure 9, Table S3) demonstrate that the intracellular levels of Gly, Ala, Val, Leu, and Lys are depleted in the Δbfd cells. Consequently, the observations made by comparing the proteomic profiles and the intracellular abundances of amino acids in the wt and Δbfd cells provide strong support for the idea that iron limitation resulting from blocking the BfrB–Bfd complex impacts carbon metabolism and the biosynthesis of amino acids derived from metabolites in the carbon and citrate cycles.

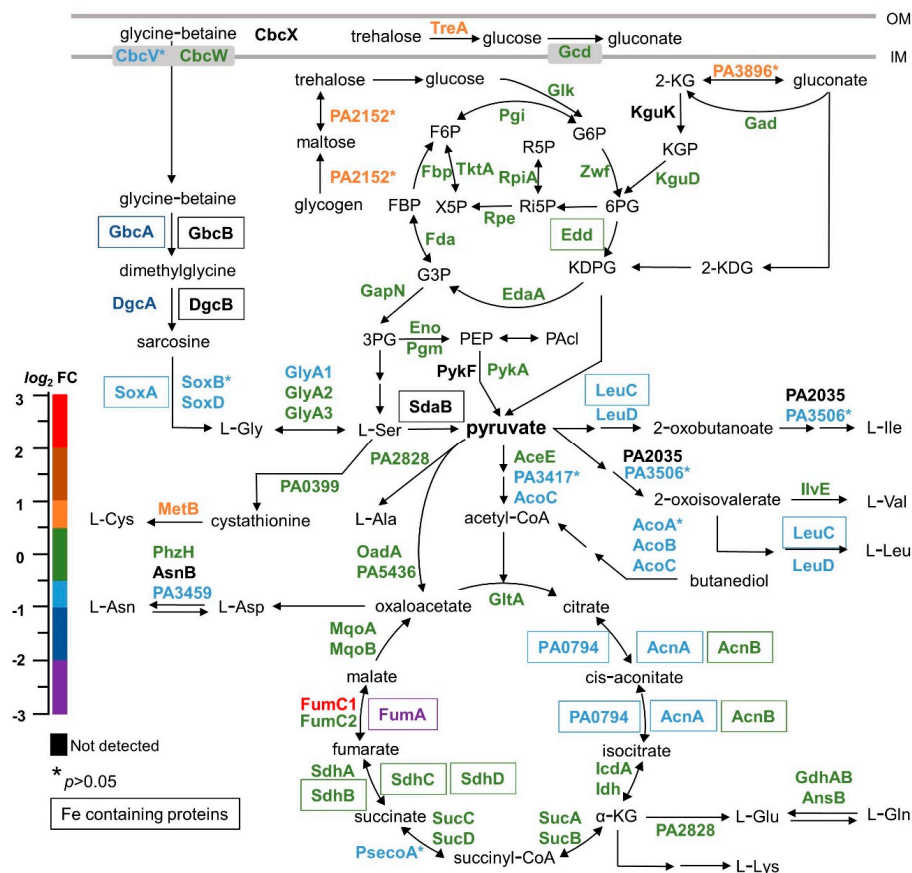


Figure 8. Proteins for carbon metabolism and for the biosynthesis of amino acids, whose skeletons are derived from the carbon and citrate cycles, are affected in the Δbfd cells. The schematic represents the main pathways of carbon metabolism and some abbreviated pathways of amino acid biosynthesis. The relative abundances (Δbfd /wt) of each of the proteins included in the scheme are color coded according to the $\log_2 FC$ scale. Enzymes that require iron to function are encased. The preparation of this scheme was aided by information from the bibliography, especially ref. [78,79]. 2-Ketogluconate (2-KG), 2-ketogluconate-6-phosphate (KGP), 2-keto-3-deoxy-D-glutamate (2-KDG), 6-phosphogluconate (6PG), ribulose-5-phosphate (Ri5P), ribose-5-phosphate (R5P), 2-keto-3-deoxy-6-phosphogluconate (KDPG), glyceraldehyde-3-phosphate (G3P), fructose-1,6-phosphate (FBP), fructose-6-phosphate (F6P).

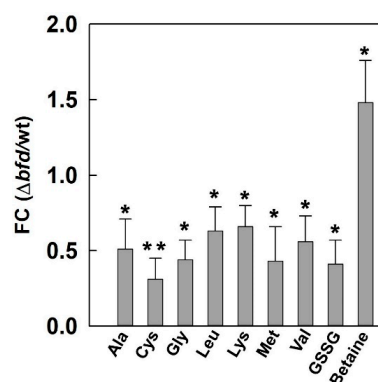


Figure 9. Amino acids derived from intermediates of the tricarboxylic acid (TCA) cycle are depleted in the Δbfd cells. NMR spectroscopy-determined intracellular levels of amino acids and other metabolites in wt and Δbfd cells are plotted as the fold change (FC) ratio Δbfd /wt. Cystine and glutathione were measured as the oxidized forms, cystine and GSSG, respectively. $p < 0.05$ denoted by * and $p < 0.01$ by **.

2.3. Inhibition of Iron Mobilization from BfrB Affects Proteins Involved in Respiration

The blockade of the BfrB–Bfd complex also affected the abundances of several proteins involved in respiration (Figure 10), including the Anr (anaerobic regulation of arginine deaminase and nitrate reduction) and Dnr (dissimilatory nitrate respiration) regulators, and proteins assembling the membrane-bound and periplasmic nitrate reductases Nar and Nap. *P. aeruginosa* is well adapted for microaerobic respiration due to its branched aerobic respiratory chain terminated by five terminal oxidases; three are cytochrome c oxidases (cbb3-1, cbb3-2 and aa3), and two are cyanide-insensitive quinol oxidases (Cyo and CIO) [87]. *P. aeruginosa* cells, which are thought to prefer microoxic conditions, have been shown to grow at concentrations of dissolved oxygen less than 3 μ M [88]. In fact, aerobically cultured *P. aeruginosa* cells block the transfer of O₂ from the gas to the liquid phase, inducing microoxic conditions for cells in exponential and stationary phase cultures [89]. Under these conditions the regulator Anr stimulates transcription of cbb3-2, and is also responsible for the start of denitrification via the regulator Dnr, although Dnr-dependent pathways are not essential at this stage [90]. In the absence of O₂, *P. aeruginosa* can use nitrate and nitrogen oxides as terminal electron acceptors. For this purpose, *P. aeruginosa* is equipped with three types of nitrate reductases: Nar, a membrane-bound enzyme expressed during anaerobic growth with nitrate as the terminal electron acceptor, Nap, a periplasmic enzyme expressed during the stationary growth phase in aerobic cultures, and Nas, a cytoplasmic enzyme which allows *P. aeruginosa* to use nitrate as a nitrogen source [87]. During anaerobic growth using nitrate for respiration, Nar and the enzymes Nir, Nor and Nos carry out the reduction of nitrate to N₂. The regulators controlling these processes include Anr, which responds to low O₂ tension, Dnr, which responds to Anr and nitric oxide (NO), and NarXL, which responds to Anr and nitrate (Figure 10A). Anr, Dnr and NarXL stimulate the transcription of the *narK1K2GHJI* operon encoding nitrate/nitrite transporters (NarK1 and NarK2) and the structural genes of Nar [91]. The *nap* operon is thought to be under the control of RpoS, and therefore it is expressed in the stationary growth phase [87].

The Anr regulatory protein is enriched in the Δbfd cells, whereas Dnr is depleted and NarXL exhibits no change relative to the wild type cells (Figure 10). A possible interpretation of these observations would suggest that the enrichment of Anr in the Δbfd cells is in response to sensing lower O₂ tension than in their wt type counterparts. The depletion of Dnr and NarI proteins, as well as the “normal” levels of NarXL, however, suggest that an alternative mechanism may be responsible for the Anr enrichment in Δbfd , whereby the iron limitation imposed by blocking the BfrB–Bfd complex causes the accumulation of inactive Anr. In this context, it is important to note that Anr is an analog of *E. coli* FNR (fumarate nitrate reductase regulator) [92]. To function as a transcriptional regulator, FNR and Anr must be in dimeric form and harboring one O₂-sensitive [4Fe-4S] cluster per subunit. Exposure to O₂ causes iron loss from the [4Fe-4S] cluster, resulting in a cluster-free enzyme that dissociates into monomers unable to bind DNA [93]. Importantly, *E. coli* cells grown aerobically have been shown to contain significant amounts of apo-FNR [94], and the apo-FNR in these cells has been shown to be relatively stable and actively recycled into a functional [4Fe-4S] dimer under iron-replete conditions [95]. As such, the enrichment of Anr in the Δbfd cells may be explained by the low iron and low sulfur (see below) conditions that slow the incorporation of iron and sulfur into [4Fe-4S] clusters in the existing and de novo synthesized Anr, causing the enzyme to accumulate in its inactive apo-form. Evidence supporting this idea was obtained from analysis of the proteomic profile in the context of Anr as a transcriptional activator of many genes in *P. aeruginosa* [96]. This analysis reveals that most of the proteins coded by genes transcriptionally activated by Anr are depleted in the Δbfd cells, despite the enrichment of Anr (Figure 10B). Consequently, these observations support the hypothesis that iron limitation caused by blocking the BfrB–Bfd complex impairs the efficient incorporation of iron sulfur clusters into recycled or de novo synthesized apo-Anr.

It is also of interest to note that among the proteins coded by genes transcriptionally activated by Anr but which are depleted in the Δbfd cells, several are iron-dependent. Hemerythrin is a di-Fe center protein thought to transport O₂ in microoxic conditions [97], HemN is a [4Fe-4S] enzyme that functions

as an O₂-independent coproporphyrinogen IX oxidase in heme biosynthesis, cytochrome *c* peroxidase (CcpR) is a di-heme enzyme thought to function in the prevention of peroxide buildup in the cell [98], and the cytoplasmic catalase KatA is a heme-containing enzyme that catalyzes peroxide decomposition into water and O₂. The transcription of the *katA* gene is driven by two promoters; *katAp1* is required in the logarithmic growth phase, and *katAp2*, which is transcriptionally activated by Anr, is required for KatA function in the stationary phase [99]. These observations suggest that the biosynthesis and maturation of these important proteins is affected by low iron and sulfur, which limits the synthesis of iron- and sulfur-containing cofactors, and by the accumulation of inactive Anr, which leads to the repression of the corresponding genes.

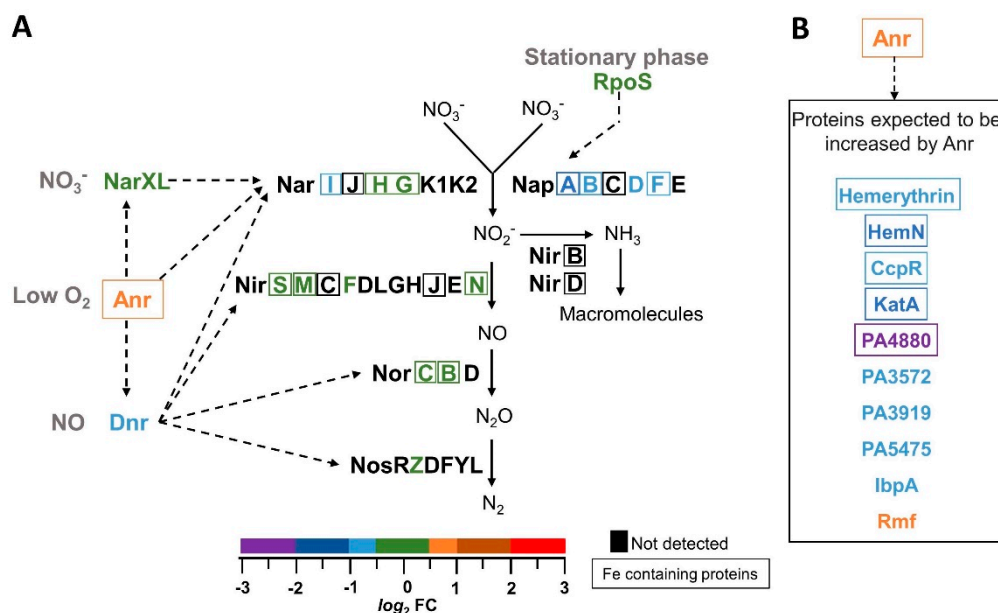


Figure 10. (A) Schematic representation of the proteins involved in the denitrification pathway. The relative abundances ($\Delta bfd/wt$) of each of the proteins in the pathway are color coded according to the $\log_2 FC$ scale; proteins that require iron to function are encased. The conditions that activate expression of the regulatory proteins Anr, Dnr, NarXL and RpoS are in gray; the segmented arrows indicate which proteins are transcribed in response to each of the regulatory proteins. The preparation of this scheme was aided significantly by ref. [100]. (B) Proteins coded by genes expected to be transcriptionally activated by Anr are depleted in the Δbfd cells, despite enrichment of Anr.

Several of the proteins encoded by the *napEFDABC* operon are also depleted in the Δbfd cells (Figure 10A). The *nap* operon codes for the periplasmic nitrate reductase (Nap) enzyme and its accessory proteins. In aerobically grown *P. aeruginosa*, Nap expression is controlled by the sigma factor RpoS during the stationary growth phase [87]. Recent work has shown that nap expression is repressed in response to phenazines via a yet-unidentified regulator, with PCA and 5-Me-PCA exerting the stronger influence [100]. The same study reported that Anr is less active in the presence of phenazines, and suggested that phenazines can alter the balance between active and inactive Anr by oxidizing the [4Fe-4S] clusters of the active enzyme. These ideas are in good agreement with the observations reported herein, whereby iron starvation induced by blocking the BfrB–Bfd complex in the Δbfd cells causes the enrichment of enzymes for the synthesis of phenazines (Figure 7A,B), as well as demonstrating high levels of PCA (Figure 7C). When this information is considered together, a model emerges wherein the elevated phenazine levels resulting from iron limitation (i) repress the *nap* operon and (ii) elevate the reduction potential of the cell, thus accelerating the oxidation of [4Fe-4S] centers, such as that in Anr. Iron limitation interferes with the efficient rebuilding of damaged [4Fe-4S] clusters,

which results in the accumulation of inactive Anr and the concomitant repression of genes that are normally transcriptionally activated by functional Anr.

These findings also suggest that it is probable that other enzymes whose functions depend on relatively sensitive [Fe-S] active centers can be affected similarly because the repair of the clusters is slowed or impeded by iron and sulfur limitation. In support of these ideas, below we present evidence suggesting that the blockade of the BfrB–Bfd complex also elicits a sulfur starvation response, which is expected to adversely affect the construction and repair of the [Fe-S] centers important for many crucial processes.

2.4. Inhibition of Iron Mobilization from BfrB Affects Assimilatory Sulfate Reduction and Sulfur Traffic

Sulfur, an essential element for bacterial life, is a component of the amino acids cysteine and methionine. *P. aeruginosa* assimilates sulfur preferentially from sulfate (SO_4^{2-}), which is imported from the environment and reduced intracellularly to sulfide (S^{2-}) for its subsequent incorporation into sulfur-containing molecules. A primary path of sulfur assimilation, the incorporation of S^{2-} into cysteine plays a crucial role in the biogenesis of [Fe-S] clusters, in the biosynthesis of antioxidant proteins and peptides, and as a precursor of methionine, coenzyme A, coenzyme M, and also thiamine, biotin, lipoic acid and the siderophore pyochelin [101,102]. Bacteria respond to sulfate or cysteine starvation by deploying the so-called sulfate starvation-induced proteins (SSI proteins), which in *P. aeruginosa* consist of sulfate and sulfonate transport systems for the uptake of sulfate and alkyl sulfonates, as well as sulfatase and sulfonatase enzymes, which function in the reduction of the sulfate and alkylsulfonate to S^{2-} for its subsequent incorporation in cysteine [103]. In this context, it is interesting that many of the SSI proteins are enriched in the Δbfd cells (Figure 11A), because it indicates that the mutant cells are deficient in sulfate or cysteine. The SSI proteins are coded by genes in the *spb*-containing *cysPTWA* operon, where Sbp is a periplasmic sulfate-binding protein, CysP is a periplasmic thiosulfate binding protein, CysT and CysW are the membrane proteins, and CysA is an ATPase. That Sbp is highly enriched whereas CysP is not suggests that the Δbfd cells are actively searching/importing SO_4^{2-} [104]. The cytoplasmatic enzymes CysD and CysN, also enriched in the mutant cells, catalyze the transformation of SO_4^{2-} , first into adenylyl sulfate (APS) and then into 3'-phosphoadenylyl sulfate (PAPS). PAPS is then transformed into sulfite (SO_3^-) by the enzyme CysH, and SO_3^- is subsequently reduced to S^{2-} by the NADPH-dependent sulfite reductase CysI, which requires siroheme and FAD to function [105]. Equally consistent with a sulfur starvation response, the proteomic data indicate the enrichment of TauA (taurine uptake) and enzymes PA3445 and PA2594, which function in the uptake of alkanesulfonates [105] (Figure 11A).

The enrichment of proteins in the sulfate starvation response in the Δbfd cells indicates that the iron limitation imposed by blocking the BfrB–Bfd complex leads to SO_4^{2-} deficiency. Given that sulfur assimilation proceeds via the reduction of SO_4^{2-} for the subsequent incorporation of a sulfur atom from S^{2-} in cysteine (and other organic molecules), the enrichment pattern suggests cysteine deficiency in the Δbfd cells. In this context, it is interesting that S^{2-} (in equilibrium with HS^- and H_2S) can be oxidized to sulfane sulfur (HS_nH ; $n \geq 1$) by a sulfide:quinone oxidoreductase enzyme [106,107]. The pertinent sulfide:quinone oxidoreductase enzyme in *P. aeruginosa* (PA2556) is depleted in the Δbfd cells (Figure 11A), an observation indicating that the Δbfd cells prioritize S^{2-} for cysteine biosynthesis. Additional evidence supporting the idea of cysteine deficiency was obtained from the NMR spectroscopic analysis, which shows that the levels of cysteine (measured as cystine) and glutathione (measured as oxidized form) in the Δbfd cells are ~30–40% of those in the wt cells (Figure 9). It is therefore clear that the iron starvation induced by blocking the BfrB–Bfd complex leads to cysteine deficiency in *P. aeruginosa*. Cysteine deficiency in the iron-starved Δbfd cells is probably a consequence of several processes, including but not restricted to: (i) the overproduction of pyochelin, which requires two cysteine molecules in its biosynthesis, (ii) the stress caused by an abundance of phenazines, such as the high-redox potential PCA, which induces oxidative stress and therefore the faster turnover and damage of sulfur-dependent oxidative stress defense molecules, such as glutathione

and thioredoxin, and (iii) the repair and de novo synthesis of [Fe-S] clusters oxidized by the abundance of high-redox potential phenazines.

Additional evidence indicating that iron starvation in the Δbfd cells affects sulfur management stems from observations regarding the biosynthesis of cofactors containing sulfur atoms, such as biotin, thiamine, and tRNA thiolation (Figure 11B). In the final step of biotin biosynthesis, the incorporation of a sulfur atom requires biotin synthase (BioB), which is enriched in the Δbfd cells. The sulfur atom incorporated into biotin is donated from a [2Fe-2S] cluster in BioB, which leads to cluster loss and inactive enzyme, followed by an iron- and sulfur-dependent repair mechanism that installs a new [2Fe-2S] cluster in BioB [108]. As such, it is possible that the iron and sulfur deficiencies in the Δbfd cells lead to an enrichment of BioB as a mixture of active and inactive forms. The enzyme PA2062, a cysteine desulfurase akin to IscS, is implicated in thiamine metabolism and is highly enriched in the Δbfd cells (Figure 11B). Some organisms have more than one copy of cysteine desulfurase, which play pivotal roles in the initial stages of sulfur trafficking within cells. These enzymes extract a sulfur atom from cysteine to form a persulfide intermediate, which is subsequently incorporated into the biosynthetic pathways leading to the formation of [Fe-S] clusters and sulfur-containing biofactors [109]. The enzyme MiaB, depleted in the Δbfd cells, catalyzes the posttranscriptional thiolation of a subset of tRNAs, a process required for their maturation. MiaB harbors two essential [4Fe-4S] clusters, which catalyze the insertion of a sulfur atom into isopentenyl adenosine to produce 2-methylthio-6-isopentenyl adenosine [110] (Figure 11B).

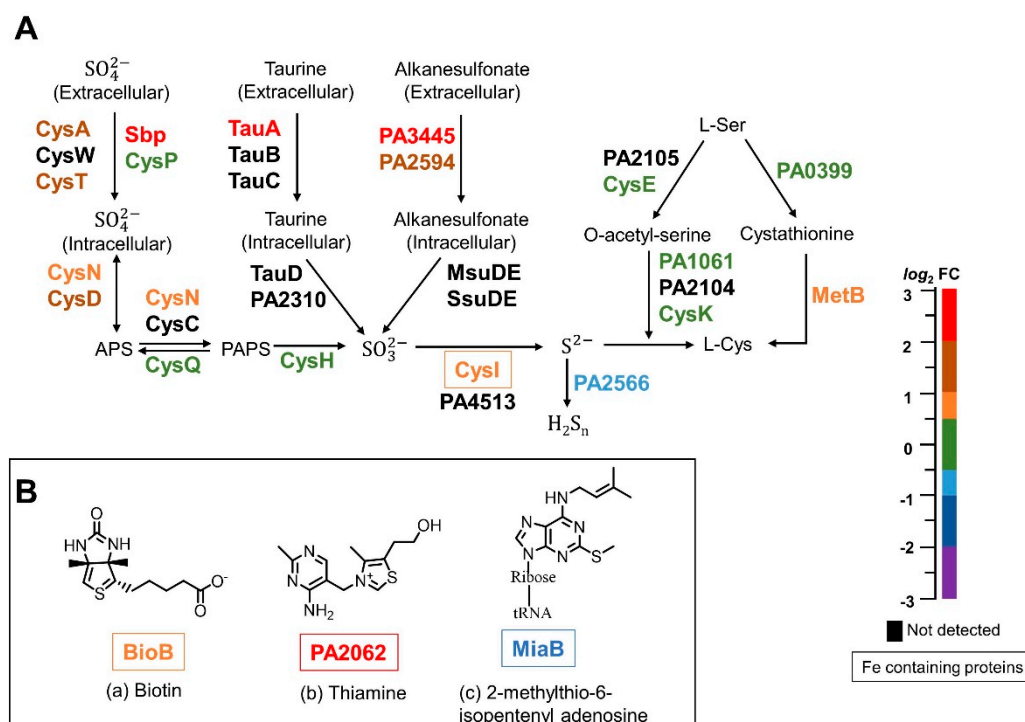


Figure 11. The sulfate starvation response proteins are enriched in the Δbfd cells. (A) Schematic representation of the sulfate starvation-induced proteins. The relative abundances ($\Delta bfd/\text{wt}$) of each of the proteins in the pathway is color coded according to the $\log_2 \text{FC}$ scale; proteins that require iron to function are enclosed. (B) Proteins for the biosynthesis of sulfur-containing cofactors are affected in the Δbfd cells.

3. Conclusions

Our work aims at introducing a new strategy for exploiting bacterial iron metabolism, the inhibition of iron mobilization from bacterioferritin. Iron mobilization from BfrB in *P. aeruginosa* requires the formation of a specific complex with Bfd (Figure 1) [27,30]. Accordingly, blocking iron mobilization

from BfrB by deletion of the *bfd* gene (Δbfd) “locks” iron in the bacterioferritin [16] and impairs biofilm formation [14]. These findings encouraged the development of novel small molecule inhibitors of the BfrB–Bfd complex, which constrain *P. aeruginosa* cell growth and potentiate the activity of the fluoroquinolone antibiotics [10]. Culturing Δbfd cells, or wt cells in the presence of an inhibitor of the BfrB–Bfd complex, leads to pyoverdine overproduction, which has been interpreted to suggest that “locking” iron in BfrB causes intracellular iron limitation [10,16]. Although pyoverdine overproduction indeed suggests iron limitation, secretion of the siderophore may occur independently of its regulation by intracellular iron levels [20], and does not per se indicate the extent of intracellular iron limitation, or if such limitation affects cellular fitness.

We conducted this work to investigate if the deletion of the *bfd* gene elicits iron homeostasis dysregulation and if the lesion in iron metabolism (Δbfd) affects metabolic homeostasis in *P. aeruginosa*. The results unequivocally show that the Δbfd cells experience severe iron limitation, as is evident not only in the overexpression of proteins involved in siderophore biosynthesis, but also in the enrichment of proteins involved in heme uptake/utilization, and AQ and phenazine biosynthesis. The analytical quantification of pyoverdine, AQs and phenazines corroborated our interpretation of the proteomic response and demonstrated that all these metabolites are produced at significantly higher levels in the Δbfd cells. In the context of the intracellular iron starvation that ensues in the Δbfd cells, it is important to underscore that the cells were cultured in iron-replete media (10 μ M Fe), so the acute iron starvation that develops in the Δbfd cells is a direct consequence of iron flowing unidirectionally into BfrB.

In addition to demonstrating global iron limitation, the proteomic profiles show that the lesion in iron metabolism caused by locking iron in BfrB adversely affects important metabolic pathways, including carbon metabolism, amino acid biosynthesis, respiration, and sulfur metabolism. Iron limitation caused by inhibiting iron mobilization from BfrB appears to affect these paths in at least two predominant ways, as follows: (i) It affects the abundance of iron-dependent proteins, which in turn affect the regulation and abundance of other proteins participating in the same metabolic pathways. (ii) It elicits an overproduction of high-potential phenazines, which induce oxidative stress and consequently damage to [Fe-S] clusters and sulfur-dependent oxidative stress defense molecules, such as glutathione and thioredoxin. The increased demand for sulfur needed to repair [Fe-S] clusters and sulfur-dependent molecules probably overwhelms the sulfur homeostasis machinery, as is suggested by the depleted levels of cysteine and glutathione in the Δbfd cells.

Finally, it is interesting to compare the findings reported herein with results from a study by Nelson et al. comparing the proteomic responses of wt *P. aeruginosa* PAO1 cells cultured in Fe-rich and Fe-deficient media [111]. It is important to underscore that in the study by Nelson et al., the cellular response to low iron was investigated by comparing the proteomic response of wt cells with intact iron homeostasis machinery cultured in high vs. low iron conditions. In comparison, in this study we compare the proteomic response of wt cells with that of Δbfd cells, which have a lesion in the iron homeostasis machinery. In addition, in this study the cells were cultured under iron-replete conditions; intracellular iron limitation in the Δbfd cells develops because intracellular iron is locked in BfrB. A comparison of the proteins detected in each of the studies and their corresponding abundances is presented in Table S2. Although in both studies iron limitation elicits the deployment of siderophores and heme acquisition/utilization systems, considering the differences observed in the two studies is insightful. In the wt cells cultured under low iron conditions (Nelson et al.), the proteins involved in sulfate and sulfonate assimilation, the reduction of the oxo-anions to sulfite and sulfide, and the biosynthesis of cysteine, are depleted [111]. In stark contrast, these proteins are enriched in the Δbfd cells (Figure 11). A second significant difference is in phenazine biosynthesis. While in the wt cells cultured in low iron conditions the proteins involved in phenazine biosynthesis are depleted [111], these proteins are enriched in the Δbfd cells (Figure 7). Considering these two significant differences supports the detrimental consequences of dysregulating iron homeostasis by blocking the BfrB–Bfd complex; the overproduction of phenazines in the Δbfd cells leads to oxidative stress, which in turn damages [Fe-S] clusters and sulfur-containing antioxidant molecules. This situation imposes

a very difficult-to-meet-demand for sulfur and iron assimilation, which ultimately results in low levels of cysteine, antioxidant molecules and sulfur- and iron-dependent molecules (Figure 9 and Table S1). These observations lead us to hypothesize that small molecule inhibitors of the BfrB–Bfd complex, by virtue of eliciting an irreversible accumulation of iron in BfrB, would trigger a homeostatic dysregulation akin to that reported here for the Δbfd cells, thus encouraging the development of inhibitors of the BfrB–Bfd complex for possible therapeutic applications.

4. Materials and Methods

4.1. Strains, Media and Growth Conditions

Chemicals were purchased from Fisher Scientific (Waltham, MA, USA) unless otherwise stated. *P. aeruginosa* (PA01) was purchased from the University of Washington Genome center (Seattle, WA, USA). The PA01-derived strain with an unmarked, in-frame deletion of the *bfd* gene (Δbfd) had been prepared previously [16]. All strains were maintained on Pseudomonas Isolation Agar (PIA, BD Biosciences, San Jose, CA, USA). *Pseudomonas aeruginosa* isolation (PI) media was used to culture cells. PI media contains 20 g L^{−1} peptone, 1.4 g L^{−1} MgCl₂·6H₂O, 10 g L^{−1} K₂SO₄, 25 mg L^{−1} irgasan (Sigma-Aldrich, St. Louis, MO, USA), and 20 mL L^{−1} glycerol, pH 7.0. PI media was supplemented with 10 μM iron using a 10 mM stock of (NH₄)₂Fe(SO₄)₂ (pH~2.0).

4.2. Cell Growth and Preparation of Lysate Solution

Pre-cultures (5 mL) of wild type (wt) and Δbfd *P. aeruginosa* cells were grown in PI media for 12 h in 50 mL conical tubes covered with an air-permeable membrane at 37 °C and 220 rpm. The cells were centrifuged at 4000 rpm for 10 min and the cell pellets washed twice with PI media not supplemented with iron. The cell pellets were resuspended in PI media supplemented with 10 μM iron, diluted in the same media to an optical density at 600 nm (OD₆₀₀) = 0.001, and 50 mL of the cell suspension was transferred to 250 mL polypropylene Erlenmeyer flasks. The flasks were covered with an air permeable membrane and incubated for 30 h at 37 °C and 230 rpm. A small volume was sampled for enumeration of viable cells prior to harvesting the cells by centrifugation (4000 rpm, 15 min and 4 °C). The cell pellets were washed twice with 10 mL of phosphate buffer saline (PBS) and stored at −20 °C overnight. The cell pellets were re-suspended in 5 mL 1% SDS in water and sonicated for 90 s in a Qsonica Q500 sonicator operating at a 20% pulse amplitude, alternating 10 s pulse-on and 10 s pulse-off. The resultant lysate solutions were stored at −20 °C until further analysis. The cell-free supernatants were analyzed for pyoverdine using a previously reported protocol [16].

4.3. Sample Preparation and Proteomics Workflow

These were carried out by following the published protocols developed at the Proteomics Core Facility, Louisiana State University Health Science Center, New Orleans [112]. Three biological replicates were conducted each for the wt and Δbfd cells. Briefly, 100 μg of protein per sample was used for trypsin digestion. The protein concentration was determined with the aid of BCA protein assay kit (Pierce, Thermo Scientific, Rockford, IL, USA) using an eight-point BSA standard curve. Proteins were reduced using 10 mM tris(carboxyethyl)phosphine (TCEP) for 1 h at 55 °C, and subsequently alkylated with 20 mM iodoacetamide for 30 min at room temperature in the dark. Proteins were subjected to chloroform-methanol precipitation, and the resultant pellet was digested with 2 μg of sequencing grade trypsin at 37 °C overnight. The next day, tryptic peptides were labeled with a TMT 6plex reagents set (Thermo Scientific) according to the manufacturer's recommended protocol. The tagged samples were stored at −80 °C until analysis. An equal volume from each TMT tagged sample was pooled into a single tube and purified using acidic reverse phase conditions (SepPak-Waters, Milford, MA, USA). Once the samples were dried, a fractionation step was carried out to lower the complexity of the sample. The sample volume was adjusted to 115 μL by 20 mM ammonium hydroxide (pH 10), and basic-pH reverse phase chromatography (Dionex U3000, Thermo Scientific, West Palm Beach, FL,

USA) was carried out according to the parameters below. The injection volume was 100 μ L, and the flow rate was 0.1 mL/min. A 90 min gradient was developed from 10 mM ammonium hydroxide (pH = 10) to 100% acetonitrile (pH = 10). A total of 48 200 μ L fractions were collected, and the fractions were re-combined in a checkerboard fashion (fraction 1, 13, 25, and 37—super fraction 1; fractions 2, 14, 26, 38—super fraction 2, etc.), resulting in 12 ‘super fractions’. These fractions were run on a Dionex U3000 nanoflow coupled to a Thermo Scientific™ Orbitrap Fusion™ Tribrid™ Mass Spectrometer (Thermo Scientific). Liquid chromatography was performed at a flow rate of 0.3 μ L/min (Trap column: C18 PepMap 100, 5 μ m, 100 Å; separation column: PicoChip REPROSIL-Pur C18-AQ, 3 μ m, 120 Å, 105 mm). A 90 min chromatographic method was employed. The gradient was as follows: 2–25% ACN in 0.1% formic acid (FA)-65 min, 50% ACN/FA-10 min, 90% ACN/FA-5 min, and re-equilibration 2% ACN/FA-10 min.

Electrospray ionization was performed at 2.6 kV. Data acquisition used an MS3 approach; survey scans were performed in the Orbitrap, using a resolution of 120,000. MS2 scans were done in the linear ion trap, using a collision-induced dissociation of 25%. For the fragmentation of the TMT-reporter ions, high-energy collision dissociation (HCD) of 65% was used and detected in the Orbitrap using a 30,000 resolution. Runs were done in triplicate for each super fraction.

TMT data were analyzed using Proteome Discoverer 2.2. The triplicate runs for the 12 super fractions were merged and searched against SEQUEST. The parameters for searching included static modifications of TMT reagents on lysine and N-terminus (+229.163), carbamidomethyl on cysteines (=57.021), and the dynamic modification of methionine oxidation (=15.9949), two maximum trypsin missed-cleavages, parent ion tolerance—10 ppm, and the fragment mass tolerance—0.6 Da. High-scoring peptides were considered using a false discovery rate of 1%. Data files were searched against the *Pseudomonas* Genome Database (www.Pseudomonas.com).

4.4. Data Analysis

A volcano plot was generated using the \log_2 (fold change) and the $-\log_{10}$ (abundance ratio *p*-values). Data were filtered based on the fold change, and the abundance ratio *p*-values. Proteins exhibiting a (Δbfd)/(wild type) fold change ≥ 1.4 and ≤ 0.7 , and the abundance ratio *p*-value < 0.05 , are considered to be differentially expressed [34]. The filtered datasets were uploaded onto the Kyoto Encyclopedia of Genes and Genomes (KEGG) Pathway Mapper and searched against *P. aeruginosa* (PA01) organism-specific pathways [113]. Identified proteins in the KEGG mapper were also searched against the *Pseudomonas* genome database (<https://www.pseudomonas.com>) and UniProt (<https://www.uniprot.org>) to obtain functional predictions and classifications [36].

4.5. NMR Analysis of Metabolites

Pseudomonas aeruginosa PAO1 cells (three biological replicates) were cultured and harvested as described above. The harvested cells were resuspended in 1.25 mL of HPLC-grade methanol (OmniSolv), incubated for 30 min at ambient temperature and then centrifuged for 30 min at 4000 rpm and 4 °C. The supernatants were transferred to separation funnels containing 1.25 mL of deionized water and then extracted with 2.5 mL of chloroform. The aqueous phase was frozen at -80 °C and freeze-dried with the aid of a SpeedVac concentrator (Thermo SAVANT, SPD111V) overnight. The dry powder was dissolved in 550 μ L of PBS (pH 7.4) prepared in D₂O (99.8%) containing 0.01% (*w/v*) 3-(Trimethylsilyl) propane-1-sulfonate, sodium salt (DSS) for chemical shift referencing. The solutions were vortexed and centrifuged and then transferred to 5 mm NMR tubes.

NMR spectra were acquired at 298 K on a Bruker Avance III 800 MHz spectrometer equipped with a 5 mm TCI cryoprobe. One-dimensional ^1H NMR spectra were acquired (128 scans) using the 1D-NOESY experiment and pre-saturation of the water peak, with a spectral width of 16,000 Hz, 65 K data point, 2.0 s acquisition time and 1.0 s relaxation delay. Spectra were apodized with a 0.3 Hz line broadening prior to Fourier transformation. ^1H - ^{13}C HSQC (heteronuclear single quantum correlation) spectra were acquired with a spectral width of 8000 Hz, 4096 data points and 1.0 s

relaxation delay in the direct-detected dimension (128 scans), and 512 data points over a spectral width of 36,000 Hz in the indirect-detected dimension. ^1H - ^1H TOCSY (total correlation spectroscopy) spectra were acquired with a spectral width of 8000 Hz, 4096 data points and 1.0 s relaxation delay (16 scans) in the direct-detected dimension, and 256 datapoints over a spectral width of 8000 Hz in the indirect-detected dimension. Adjustments to the baseline, peak phasing and chemical shift referencing were made using Bruker Topspin 3.6.2. To identify the identity of metabolites, the chemical shifts in the NMR spectra were compared to the Biological Magnetic Resonance Database [114] and the Human Metabolome Database [115] for positive matches. To corroborate metabolite identifications the chemical shifts were correlated using the ^1H - ^{13}C HSQC and the ^1H - ^1H TOCSY spectra (Table S3). Combining the information from the 1D and 2D NMR spectra greatly reduced the ambiguity of assigning chemical shifts to metabolites. The volumes of judiciously chosen peaks in the ^1H - ^{13}C HSQC spectra were integrated and used to compare the relative levels of metabolites in the wt and Δbfd cells. The average and standard deviations obtained from 3 biological replicates have been summarized in Figure 9. The statistical significance between the means and standard deviations of values comparing the levels of metabolites in the wt and Δbfd cells was determined using Student's *t* test with the aid of SigmaPlot (Systat Software, Inc. San Jose, CA, USA).

4.6. Analysis of 2-Alkyl-4-Quinolones (AQs)

The HHQ, PQS and HQNO extracted from bacterial cells and cell culture supernatants were quantitated with the aid of liquid chromatography—mass spectrometry using a previously described method [14]. In brief: For the analysis of AQs in bacterial cells, a 1.0 mL sample of bacterial cell culture was centrifuged and the cell pellets resuspended in 3 mL HPLC-grade methanol. For the analysis in spent media, 3 mL of cell culture were clarified by centrifugation. The solutions were acidified with 15 μL 12 N HCl, extracted into 6 mL of ethyl acetate and incubated at ambient temperature for 1 h with slow shaking. The organic layers were separated by centrifugation, transferred to new microcentrifuge tubes, and evaporated overnight using a SpeedVac Concentrator. Quantitative analysis was performed using an LC-MS system comprising an Agilent 1260 Infinity II HPLC and an Agilent 6230 time-of-flight mass spectrometer operating in the positive ion mode with a capillary voltage of 4000 V, end plate voltage of 150 V, and nebulizing gas (N_2) temperature of 325 $^\circ\text{C}$. Samples were separated in a Poroshell 120 EC-C8 column (3.0 \times 100 mm, 2.7 μm particle size, 120 \AA pore size; Agilent) with a 0.4 mL/min flow rate and the following gradient: 97% A (2 min), 63% A (5 min), 57% A (21 min), and 3% A (31 min), revert to the initial conditions and equilibrate for 11 min; A: 0.1% formic acid in water. B: 0.1% formic acid in acetonitrile. AQs were detected using full scan mode (m/z 130 to 350) and quantitated by measuring the integrated peak area of the corresponding $[\text{M} + \text{H}]^+$ ions and a standard curve constructed from commercially available HHQ, HQNO, and PQS.

4.7. Analysis of Phenazine 1-Carboxylic Acid (PCA) and Pyocyanin (PYO)

The cell suspension (3 mL) was acidified to pH 4.0 with HCl prior to extraction with 6 mL of ethyl acetate. The ethyl acetate extracts were kept at room temperature for 30 min with gentle shaking prior to centrifugation at 4 $^\circ\text{C}$ and 4000 rpm for 10 min. The ethyl acetate layer was transferred to new microcentrifuge tubes and evaporated with the aid of a Speed Vac Concentrator. Dried samples were resuspended in 300 μL of methanol and stored at $-20\text{ }^\circ\text{C}$. Quantitative determination was carried out by LC-MS using an Agilent 6230 TOF Ms (see above) in the positive ion mode. Samples were separated in a Poroshell 120 EC-C18 column (2.1 \times 100 mm, 2.7 μm particle size, 120 \AA pore size; Agilent) using a flow rate of 0.4 mL/min and the following gradient: 95% A (2 min), 40% A (11 min), 5% A (26 min), and reequilibration to initial conditions (11 min); A = 0.1% formic acid in water, B = 0.1% formic acid in acetonitrile. Phenazines were detected using full scan mode (m/z 130 to 350) and quantitated by measuring the integrated peak area of the corresponding $[\text{M} + \text{H}]^+$ ions and a standard curve constructed using commercially available PCA (Evo Blocks Ltd., Budapest, Hungary) and PYO (Cayman Chemical, Ann Arbor, MI, USA).

Supplementary Materials: The following are available online at <http://www.mdpi.com/2076-0817/9/12/980/s1>. Figure S1: Growth curves and levels of pyoverdine secreted by wt and Δbld *P. aeruginosa* cells; Table S1: Proteins exhibiting significant abundant differences between wt and Δbld cells; Table S2: Proteins exhibiting significant abundance differences between wt and Δbld cells compared to proteins exhibiting significant abundance differences between wt cells cultured in high vs. low iron conditions; Table S3: Resonance assignments for ^1H and ^{13}C chemical shifts of amino acids and other metabolites identified by NMR spectroscopy in the wt and Δbld cells.

Author Contributions: Conceptualization, A.N.D.P.H., L.F. and M.R.; investigation, A.N.D.P.H., L.F. and M.R.; methodology, J.G., T.W. and A.K.M., F.D., A.N.D.P.H. and L.F. writing—original draft preparation, M.R.; writing—review and editing A.N.D.P.H., L.F. and M.R.; project administration, M.R.; funding acquisition, M.R. All authors have read and agreed to the published version of the manuscript.

Funding: This research was funded by grants from the National Institutes of Health (AI1225529) and the National Science Foundation (MCB1837877) to M.R.

Acknowledgments: A portion of this work was performed in the McKnight Brain Institute at the National High Magnetic Field Laboratory's Advanced Magnetic Resonance Imaging and Spectroscopy (AMRIS) Facility, which is supported by National Science Foundation Cooperative Agreement No. DMR-1644779 and the State of Florida.

Conflicts of Interest: The authors declare no conflict of interest. The funders had no role in the design of the study, in the collection, analyses, or interpretation of data, in writing the manuscript, or in the decision to publish the results.

References

- Horcajada, J.P.; Montero, M.; Oliver, A.; Sorli, L.; Luque, S.; Gomez-Zorrilla, S.; Benito, N.; Grau, S. Epidemiology and Treatment of Multidrug-Resistant and Extensively Drug-Resistant *Pseudomonas aeruginosa* Infections. *Clin. Microbiol. Rev.* **2019**, *32*. [CrossRef] [PubMed]
- Burrows, L.L. The Therapeutic Pipeline for *Pseudomonas aeruginosa* Infections. *ACS Infect. Dis.* **2018**, *4*, 1041–1047. [CrossRef] [PubMed]
- Oliver, A.; Mulet, X.; López-Causapé, C.J. The increasing threat of *Pseudomonas aeruginosa* high-risk clones. *Drug Resist. Updates* **2015**, *21–22*, 41–59. [CrossRef] [PubMed]
- Taconelli, E.; Carrara, E.; Savoldi, A.; Harbarth, S.; Mendelson, M.; Monnet, D.L.; Pulcini, C.; Kahlmeter, G.; Kluytmans, J.; Carmeli, Y.; et al. Discovery, research, and development of new antibiotics: The WHO priority list of antibiotic-resistant bacteria and tuberculosis. *Lancet Infect. Dis.* **2018**, *18*, 318–327. [CrossRef]
- Chellat, M.F.; Raguz, L.; Riedl, R. Targeting Antibiotic Resistance. *Angew. Chem. Int. Ed. Engl.* **2016**, *55*, 6600–6626. [CrossRef]
- Lakemeyer, M.; Zhao, W.; Mandl, F.A.; Hammann, P.; Sieber, S.A. Thinking Outside the Box—Novel Antibacterials To Tackle the Resistance Crisis. *Angew. Chem. Int. Ed. Engl.* **2018**, *57*, 14440–14475. [CrossRef]
- Verderosa, A.D.; Totsika, M.; Fairfull-Smith, K.E. Bacterial Biofilm Eradication Agents: A Current Review. *Front. Chem.* **2019**, *7*, 824. [CrossRef]
- Ballouche, M.; Cornelis, P.; Baysse, C. Iron Metabolism: A Promising Target for Antibacterial strategies. *Recent Pat. Anti-Infect. Drug Discov.* **2009**, *4*, 190–205. [CrossRef]
- Foley, T.L.; Simeonov, A. Targeting iron assimilation to develop new antibacterials. *Expert Opin. Drug Discov.* **2012**, *7*, 831–847. [CrossRef]
- Punchi Hewage, A.N.D.; Yao, H.; Nammalwar, B.; Gnanasekaran, K.K.; Lovell, S.; Bunce, R.A.; Eshelman, K.; Phaniraj, S.M.; Lee, M.M.; Peterson, B.R.; et al. Small Molecule Inhibitors of the BfrB-Bfd Interaction Decrease *Pseudomonas aeruginosa* Fitness and Potentiate Fluoroquinolone Activity. *J. Am. Chem. Soc.* **2019**, *141*, 8171–8184. [CrossRef] [PubMed]
- Goss, C.H.; Kaneko, Y.; Khuu, L.; Anderson, G.D.; Ravishankar, S.; Aitken, M.L.; Lechtzin, N.; Zhou, G.; Czyz, D.M.; McLean, K. Gallium disrupts bacterial iron metabolism and has therapeutic effects in mice and humans with lung infections. *Sci. Transl. Med.* **2018**, *10*, eaat7520. [CrossRef] [PubMed]
- Heinzl, G.A.; Huang, W.; Yu, W.; Giardina, B.J.; Zhou, Y.; MacKerell, A.D., Jr.; Wilks, A.; Xue, F. Iminoguanidines as Allosteric Inhibitors of the Iron-Regulated Heme Oxygenase (HemO) of *Pseudomonas aeruginosa*. *J. Med. Chem.* **2016**, *59*, 6929–6942. [CrossRef] [PubMed]
- Post, S.J.; Shapiro, J.A.; Wuest, W.M. Connecting iron acquisition and biofilm formation in the ESKAPE pathogens as a strategy for combatting antibiotic resistance. *Medchemcomm* **2019**, *10*, 505–512. [CrossRef] [PubMed]

14. Soldano, A.; Yao, H.; Chandler, J.R.; Rivera, M. Inhibiting Iron Mobilization from Bacterioferritin in *Pseudomonas aeruginosa* Impairs Biofilm Formation Irrespective of Environmental Iron Availability. *ACS Infect. Dis.* **2020**, *6*, 447–458. [[CrossRef](#)] [[PubMed](#)]
15. Bullen, J.J.; Rogers, H.J.; Spalding, P.B.; Ward, C.G. Iron and Infection: The Heart of the Matter. *FEMS Immunol. Med. Microbiol.* **2005**, *43*, 325–330. [[CrossRef](#)] [[PubMed](#)]
16. Eshelman, K.; Yao, H.; Punchi Hewage, A.N.D.; Deay, J.J.; Chandler, J.R.; Rivera, M. Inhibiting the BfrB:Bfd Interaction in *Pseudomonas aeruginosa* Causes Irreversible Iron Accumulation in Bacterioferritin and Iron Deficiency in the Bacterial Cell. *Metallomics* **2017**, *9*, 646–659. [[CrossRef](#)]
17. Keyer, K.; Imlay, J.A. Superoxide Accelerates DNA-Damage by Elevating Free-Iron Levels. *Proc. Natl. Acad. Sci. USA* **1996**, *93*, 13635–13649. [[CrossRef](#)]
18. Mislin, G.L.; Schalk, I.J. Siderophore-dependent iron uptake systems as gates for antibiotic Trojan horse strategies against *Pseudomonas aeruginosa*. *Metallomics* **2014**, *6*, 408–420. [[CrossRef](#)]
19. Ji, C.; Miller, P.A.; Miller, M.J. Iron transport-mediated drug delivery: Practical syntheses and in vitro antibacterial studies of tris-catecholate siderophore-aminopenicillin conjugates reveals selectively potent antipseudomonal activity. *J. Am. Chem. Soc.* **2012**, *134*, 9898–9901. [[CrossRef](#)]
20. Kang, D.; Kirienko, N.V. Interdependence between iron acquisition and biofilm formation in *Pseudomonas aeruginosa*. *J. Microbiol.* **2018**, *56*, 449–457. [[CrossRef](#)]
21. O'May, C.Y.; Sanderson, K.; Roddam, L.F.; Kirov, S.M.; Reid, D.W. Iron-binding compounds impair *Pseudomonas aeruginosa* biofilm formation, especially under anaerobic conditions. *J. Med. Microbiol.* **2009**, *58*, 765–773. [[CrossRef](#)] [[PubMed](#)]
22. Moreau-Marquis, S.; O'Toole, G.A.; Stanton, B.A. Tobramycin and FDA-approved iron chelators eliminate *Pseudomonas aeruginosa* biofilms on cystic fibrosis cells. *Am. J. Respir. Cell Mol. Biol.* **2009**, *41*, 305–313. [[CrossRef](#)] [[PubMed](#)]
23. Banin, E.; Brady, K.M.; Greenberg, E.P. Chelator-induced dispersal and killing of *Pseudomonas aeruginosa* cells in a biofilm. *Appl. Environ. Microbiol.* **2006**, *72*, 2064–2069. [[CrossRef](#)] [[PubMed](#)]
24. Centola, G.; Deredge, D.J.; Hom, K.; Ai, Y.; Dent, A.T.; Xue, F.; Wilks, A. Gallium(III)-Salophen as a Dual Inhibitor of *Pseudomonas aeruginosa* Heme Sensing and Iron Acquisition. *ACS Infect. Dis.* **2020**, *6*, 2073–2085. [[CrossRef](#)] [[PubMed](#)]
25. Kaneko, Y.; Thoendel, M.; Olakanmi, O.; Britigan, B.E.; Singh, P.K. The Transition Metal Gallium Disrupts *Pseudomonas aeruginosa* Iron Metabolism and has Antimicrobial and Antibiofilm Activity. *J. Clin. Investig.* **2007**, *117*, 877–887. [[CrossRef](#)] [[PubMed](#)]
26. Minandri, F.; Bonchi, C.; Frangipani, E.; Imperi, F.; Visca, P. Promises and failures of gallium as an antibacterial agent. *Future Microbiol.* **2014**, *9*, 379–397. [[CrossRef](#)] [[PubMed](#)]
27. Rivera, M. Bacterioferritin: Structure, Dynamics and Protein-Protein Interactions at Play in Iron Storage and Mobilization. *Acc. Chem. Res.* **2017**, *50*, 331–340. [[CrossRef](#)]
28. Yao, H.; Jepkorir, G.; Lovell, S.; Nama, P.V.; Weeratunga, S.K.; Battaille, K.P.; Rivera, M. Two Distinct Ferritin-Like Molecules in *P. aeruginosa*: The Product of the *bfrA* Gene is a Bacterial Ferritin (FtnA) not a bacterioferritin (Bfr). *Biochemistry* **2011**, *50*, 5236–5248. [[CrossRef](#)]
29. Weeratunga, S.; Lovell, S.; Yao, H.; Battaille, K.P.; Fischer, C.J.; Gee, C.E.; Rivera, M. Structural Studies of Bacterioferritin B (BfrB) from *Pseudomonas aeruginosa* Suggest a Gating Mechanism for Iron Uptake via the Ferroxidase Center. *Biochemistry* **2010**, *49*, 1160–1175. [[CrossRef](#)]
30. Yao, H.; Wang, Y.; Lovell, S.; Kumar, R.; Ruvinsky, A.M.; Battaille, K.P.; Vakser, I.A.; Rivera, M. The Structure of the BfrB-Bfd Complex Reveals Protein-Protein Interactions Enabling Iron Release from Bacterioferritin. *J. Am. Chem. Soc.* **2012**, *134*, 13470–13481. [[CrossRef](#)]
31. Banin, E.; Vasil, M.L.; Greenberg, E.P. Iron and *Pseudomonas aeruginosa* biofilm formation. *Proc. Natl. Acad. Sci. USA* **2005**, *102*, 11076–11081. [[CrossRef](#)] [[PubMed](#)]
32. Thompson, A.; Schafer, J.; Kuhn, K.; Kienle, S.; Schwarz, J.; Schmidt, G.; Neumann, T.; Johnstone, R.; Mohammed, A.K.; Hamon, C. Tandem mass tags: A novel quantification strategy for comparative analysis of complex protein mixtures by MS/MS. *Anal. Chem.* **2003**, *75*, 1895–1904. [[CrossRef](#)]
33. Labaer, J.; Qiu, Q.; Anumanthan, A.; Mar, W.; Zuo, D.; Murthy, T.V.; Taycher, H.; Halleck, A.; Hainsworth, E.; Lory, S.; et al. The *Pseudomonas aeruginosa* PA01 gene collection. *Genome Res.* **2004**, *14*, 2190–2200. [[CrossRef](#)] [[PubMed](#)]

34. King, C.D.; Singh, D.; Holden, K.; Govan, A.B.; Keith, S.; Ghazi, A.; Robinson, R.A. Dataset of proteomics analysis of aging *C. elegans* exposed to *Pseudomonas aeruginosa* strain PA01. *Data Brief* **2017**, *11*, 245–251. [[CrossRef](#)] [[PubMed](#)]
35. Kanehisa, M.; Goto, S.; Sato, Y.; Kawashima, M.; Furumichi, M.; Tanabe, M. Data, information, knowledge and principle: Back to metabolism in KEGG. *Nucleic Acids Res.* **2014**, *42*, D199–D205. [[CrossRef](#)]
36. Winsor, G.L.; Griffiths, E.J.; Lo, R.; Dhillon, B.K.; Shay, J.A.; Brinkman, F.S. Enhanced annotations and features for comparing thousands of *Pseudomonas* genomes in the *Pseudomonas* genome database. *Nucleic Acids Res.* **2016**, *44*, D646–D653. [[CrossRef](#)]
37. Apweiler, R.; Bairoch, A.; Wu, C.H.; Barker, W.C.; Boeckmann, B.; Ferro, S.; Gasteiger, E.; Huang, H.; Lopez, R.; Magrane, M.; et al. UniProt: The Universal Protein knowledgebase. *Nucleic Acids Res.* **2004**, *32*, D115–D119. [[CrossRef](#)]
38. Schalk, I.J.; Guillon, L. Pyoverdine biosynthesis and secretion in *Pseudomonas aeruginosa*: Implications for metal homeostasis. *Environ. Microbiol.* **2013**, *15*, 1661–1673. [[CrossRef](#)]
39. Meyer, J.M.; Stintzi, A.; De Vos, D.; Cornelis, P.; Tappe, R.; Taraz, K.; Budzikiewicz, H. Use of siderophores to type pseudomonads: The three *Pseudomonas aeruginosa* pyoverdine systems. *Microbiology* **1997**, *143 Pt 1*, 35–43. [[CrossRef](#)]
40. Visca, P.; Imperi, F.; Lamont, I.L. Pyoverdine siderophores: From biogenesis to biosignificance. *Trends Microbiol.* **2007**, *15*, 22–30. [[CrossRef](#)]
41. Ringel, M.T.; Bruser, T. The biosynthesis of pyoverdines. *Microb. Cell* **2018**, *5*, 424–437. [[CrossRef](#)] [[PubMed](#)]
42. Hannauer, M.; Schafer, M.; Hoegy, F.; Gizzi, P.; Wehrung, P.; Mislin, G.L.; Budzikiewicz, H.; Schalk, I.J. Biosynthesis of the pyoverdine siderophore of *Pseudomonas aeruginosa* involves precursors with a myristic or a myristoleic acid chain. *FEBS Lett.* **2012**, *586*, 96–101. [[CrossRef](#)]
43. Brillet, K.; Ruffenach, F.; Adams, H.; Journet, L.; Gasser, V.; Hoegy, F.; Guillon, L.; Hannauer, M.; Page, A.; Schalk, I.J. An ABC transporter with two periplasmic binding proteins involved in iron acquisition in *Pseudomonas aeruginosa*. *ACS Chem. Biol.* **2012**, *7*, 2036–2045. [[CrossRef](#)] [[PubMed](#)]
44. Imperi, F.; Tiburzi, F.; Visca, P. Molecular basis of pyoverdine siderophore recycling in *Pseudomonas aeruginosa*. *Proc. Natl. Acad. Sci. USA* **2009**, *106*, 20440–20445. [[CrossRef](#)]
45. Hannauer, M.; Yeterian, E.; Martin, L.W.; Lamont, I.L.; Schalk, I.J. An efflux pump is involved in secretion of newly synthesized siderophore by *Pseudomonas aeruginosa*. *FEBS Lett.* **2010**, *584*, 4751–4755. [[CrossRef](#)] [[PubMed](#)]
46. Adams, H.; Zeder-Lutz, G.; Schalk, I.; Pattus, F.; Celia, H. Interaction of TonB with the outer membrane receptor FpvA of *Pseudomonas aeruginosa*. *J. Bacteriol.* **2006**, *188*, 5752–5761. [[CrossRef](#)] [[PubMed](#)]
47. Poole, K.; Neshat, S.; Krebs, K.; Heinrichs, D.E. Cloning and nucleotide sequence analysis of the ferripyoverdine receptor gene fpvA of *Pseudomonas aeruginosa*. *J. Bacteriol.* **1993**, *175*, 4597–4604. [[CrossRef](#)]
48. Ganne, G.; Brillet, K.; Basta, B.; Roche, B.; Hoegy, F.; Gasser, V.; Schalk, I.J. Iron Release from the Siderophore Pyoverdine in *Pseudomonas aeruginosa* Involves Three New Actors: FpvC, FpvG, and FpvH. *ACS Chem. Biol.* **2017**, *12*, 1056–1065. [[CrossRef](#)]
49. Gaille, C.; Reimmann, C.; Haas, D. Isochorismate synthase (PchA), the first and rate-limiting enzyme in salicylate biosynthesis of *Pseudomonas aeruginosa*. *J. Biol. Chem.* **2003**, *278*, 16893–16898. [[CrossRef](#)]
50. Schalk, I.J.; Rigouin, C.; Godet, J. An overview of siderophore biosynthesis among fluorescent Pseudomonads and new insights into their complex cellular organization. *Environ. Microbiol.* **2020**, *22*, 1447–1466. [[CrossRef](#)]
51. Serino, L.; Reimmann, C.; Visca, P.; Beyeler, M.; Chiesa, V.D.; Haas, D. Biosynthesis of pyochelin and dihydroaeruginic acid requires the iron-regulated pchDCBA operon in *Pseudomonas aeruginosa*. *J. Bacteriol.* **1997**, *179*, 248–257. [[CrossRef](#)] [[PubMed](#)]
52. Reimmann, C.; Patel, H.M.; Walsh, C.T.; Haas, D. PchC thioesterase optimizes nonribosomal biosynthesis of the peptide siderophore pyochelin in *Pseudomonas aeruginosa*. *J. Bacteriol.* **2004**, *186*, 6367–6373. [[CrossRef](#)] [[PubMed](#)]
53. Ronnebaum, T.A.; Lamb, A.L. Nonribosomal peptides for iron acquisition: Pyochelin biosynthesis as a case study. *Curr. Opin. Struct. Biol.* **2018**, *53*, 1–11. [[CrossRef](#)]
54. Huang, W.; Wilks, A. Extracellular Heme Uptake and the Challenge of Bacterial Cell Membranes. *Annu. Rev. Biochem.* **2017**, *86*, 799–823. [[CrossRef](#)]
55. Benson, D.R.; Rivera, M. Heme Uptake and Metabolism in Bacteria. *Met. Ions Life Sci.* **2013**, *12*, 279–332. [[CrossRef](#)] [[PubMed](#)]

56. Lansky, I.B.; Lukat-Rodgers, G.S.; Block, D.; Rodgers, K.R.; Ratliff, M.; Wilks, A. The cytoplasmic heme-binding protein (PhuS) from the heme uptake system of *Pseudomonas aeruginosa* is an intracellular heme-trafficking protein to the delta-regioselective heme oxygenase. *J. Biol. Chem.* **2006**, *281*, 13652–13662. [[CrossRef](#)] [[PubMed](#)]
57. Caignan, G.A.; Deshmukh, R.; Wilks, A.; Zeng, Y.; Huang, H.; Moënné-Loccoz, P.; Bunce, R.A.; Eastman, M.A.; Rivera, M. Oxidation of Heme to β - and δ -biliverdin by *Pseudomonas aeruginosa* Heme Oxygenase as a Consequence of an Unusual Seating of the Heme. *J. Am. Chem. Soc.* **2002**, *124*, 14879–14892. [[CrossRef](#)] [[PubMed](#)]
58. Winsor, G.L.; Lam, D.K.; Fleming, L.; Lo, R.; Whiteside, M.D.; Yu, N.Y.; Hancock, R.E.; Brinkman, F.S. Pseudomonas Genome Database: Improved comparative analysis and population genomics capability for Pseudomonas genomes. *Nucleic Acids Res.* **2011**, *39*, D596–D600. [[CrossRef](#)]
59. Heeb, S.; Fletcher, M.P.; Chhabra, S.R.; Diggle, S.P.; Williams, P.; Camara, M. Quinolones: From antibiotics to autoinducers. *FEMS Microbiol. Rev.* **2011**, *35*, 247–274. [[CrossRef](#)]
60. Hazan, R.; He, J.; Xiao, G.; Dekimpe, V.; Apidianakis, Y.; Lesic, B.; Astrakas, C.; Deziel, E.; Lepine, F.; Rahme, L.G. Homeostatic interplay between bacterial cell-cell signaling and iron in virulence. *PLoS Pathog.* **2010**, *6*, e1000810. [[CrossRef](#)]
61. Ochsner, U.A.; Wilderman, P.J.; Vasil, A.I.; Vasil, M.L. GeneChip Expression Analysis of the Iron Starvation Response in *Pseudomonas Aeruginosa*: Identification of Novel Pyoverdine Biosynthesis Genes. *Mol. Microbiol.* **2002**, *45*, 1277–1287. [[CrossRef](#)]
62. Oglesby, A.G.; Farrow, J.M.; Lee, J.-H.; Tomaras, A.P.; Greenbergh, E.P.; Pasci, E. The Influence of Iron on *Pseudomonas aeruginosa* Physiology A regulatory Link between Iron and Quorum sensing. *J. Biol. Chem.* **2008**, *283*, 15558–15567. [[CrossRef](#)]
63. Reinhart, A.A.; Powell, D.A.; Nguyen, A.T.; O'Neill, M.; Djapgne, L.; Wilks, A.; Ernst, R.K.; Oglesby-Sherrouse, A.G. The prrF-encoded small regulatory RNAs are required for iron homeostasis and virulence of *Pseudomonas aeruginosa*. *Infect. Immun.* **2015**, *83*, 863–875. [[CrossRef](#)] [[PubMed](#)]
64. Witzgall, F.; Depke, T.; Hoffmann, M.; Empting, M.; Bronstrup, M.; Muller, R.; Blankenfeldt, W. The Alkylquinolone Repertoire of *Pseudomonas aeruginosa* is Linked to Structural Flexibility of the FabH-like 2-Heptyl-3-hydroxy-4(1H)-quinolone (PQS) Biosynthesis Enzyme PqsBC. *Chembiochem* **2018**, *19*, 1531–1544. [[CrossRef](#)] [[PubMed](#)]
65. Rampioni, G.; Falcone, M.; Heeb, S.; Frangipani, E.; Fletcher, M.P.; Dubern, J.F.; Visca, P.; Leoni, L.; Camara, M.; Williams, P. Unravelling the Genome-Wide Contributions of Specific 2-Alkyl-4-Quinolones and PqsE to Quorum Sensing in *Pseudomonas aeruginosa*. *PLoS Pathog.* **2016**, *12*, e1006029. [[CrossRef](#)] [[PubMed](#)]
66. Knoten, C.A.; Wells, G.; Coleman, J.P.; Pesci, E.C. A conserved suppressor mutation in a tryptophan auxotroph results in dysregulation of *Pseudomonas* quinolone signal synthesis. *J. Bacteriol.* **2014**, *196*, 2413–2422. [[CrossRef](#)]
67. Mavrodi, D.V.; Bonsall, R.F.; Delaney, S.M.; Soule, M.J.; Phillips, G.; Thomashow, L.S. Functional analysis of genes for biosynthesis of pyocyanin and phenazine-1-carboxamide from *Pseudomonas aeruginosa* PAO1. *J. Bacteriol.* **2001**, *183*, 6454–6465. [[CrossRef](#)]
68. Bilal, M.; Guo, S.; Iqbal, H.M.N.; Hu, H.; Wang, W.; Zhang, X. Engineering *Pseudomonas* for phenazine biosynthesis, regulation, and biotechnological applications: A review. *World J. Microbiol. Biotechnol.* **2017**, *33*, 191. [[CrossRef](#)]
69. Deziel, E.; Gopalan, S.; Tampakaki, A.P.; Lepine, F.; Padfield, K.E.; Saucier, M.; Xiao, G.; Rahme, L.G. The contribution of MvfR to *Pseudomonas aeruginosa* pathogenesis and quorum sensing circuitry regulation: Multiple quorum sensing-regulated genes are modulated without affecting lasRI, rhlRI or the production of N-acyl-L-homoserine lactones. *Mol. Microbiol.* **2005**, *55*, 998–1014. [[CrossRef](#)]
70. Recinos, D.A.; Sekedat, M.D.; Hernandez, A.; Cohen, T.S.; Sakhtah, H.; Prince, A.S.; Price-Whelan, A.; Dietrich, L.E. Redundant phenazine operons in *Pseudomonas aeruginosa* exhibit environment-dependent expression and differential roles in pathogenicity. *Proc. Natl. Acad. Sci. USA* **2012**, *109*, 19420–19425. [[CrossRef](#)]
71. Morales, D.K.; Jacobs, N.J.; Rajamani, S.; Krishnamurthy, M.; Cubillos-Ruiz, J.R.; Hogan, D.A. Antifungal mechanisms by which a novel *Pseudomonas aeruginosa* phenazine toxin kills *Candida albicans* in biofilms. *Mol. Microbiol.* **2010**, *78*, 1379–1392. [[CrossRef](#)] [[PubMed](#)]

72. Matthijs, S.; Koedam, N.; Cornelis, P.; De Greve, H. The trehalose operon of *Pseudomonas fluorescens* ATCC 17400. *Res. Microbiol.* **2000**, *151*, 845–851. [\[CrossRef\]](#)
73. Nishimoto, T.; Nakano, M.; Shoji, I.; Chaen, H.; Fukuda, S.; Sugimoto, T.; Kurimoto, M.; Tsujisaka, Y. Existence of a Novel Enzyme Converting Maltose into Trehalose. *Biosci. Biotech. Biochem.* **1995**, *59*, 2189–2190. [\[CrossRef\]](#)
74. Tsusaki, K.; Nishimoto, T.; Nakada, T.; Kubota, M.; Chaen, H.; Sugimoto, T.; Kurimoto, M. Cloning and sequencing of trehalose synthase gene from *Pimelobacter* sp. R48. *Biochim. Biophys. Acta* **1996**, *1290*, 1–3. [\[CrossRef\]](#)
75. Preiss, J. Bacterial glycogen synthesis and its regulation. *Annu. Rev. Microbiol.* **1984**, *38*, 419–458. [\[CrossRef\]](#) [\[PubMed\]](#)
76. Park, K.-H. Roles of Enzymes in Glycogen Metabolism and Degradation in *Escherichia coli*. *J. Appl. Glycosci.* **2015**, *62*, 37–45. [\[CrossRef\]](#)
77. Jones, S.A.; Jorgensen, M.; Chowdhury, F.Z.; Rodgers, R.; Hartline, J.; Leatham, M.P.; Struve, C.; Krogfelt, K.A.; Cohen, P.S.; Conway, T. Glycogen and maltose utilization by *Escherichia coli* O157:H7 in the mouse intestine. *Infect. Immun.* **2008**, *76*, 2531–2540. [\[CrossRef\]](#) [\[PubMed\]](#)
78. Wilson, W.A.; Roach, P.J.; Montero, M.; Baroja-Fernandez, E.; Munoz, F.J.; Eydallin, G.; Viale, A.M.; Pozueta-Romero, J. Regulation of glycogen metabolism in yeast and bacteria. *FEMS Microbiol. Rev.* **2010**, *34*, 952–985. [\[CrossRef\]](#)
79. Nikel, P.I.; Chavarria, M.; Fuhrer, T.; Sauer, U.; de Lorenzo, V. *Pseudomonas putida* KT2440 Strain Metabolizes Glucose through a Cycle Formed by Enzymes of the Entner-Doudoroff, Embden-Meyerhof-Parnas, and Pentose Phosphate Pathways. *J. Biol. Chem.* **2015**, *290*, 25920–25932. [\[CrossRef\]](#)
80. Sasnow, S.S.; Wei, H.; Aristilde, L. Bypasses in intracellular glucose metabolism in iron-limited *Pseudomonas putida*. *Microbiologyopen* **2016**, *5*, 3–20. [\[CrossRef\]](#)
81. Liu, Q.; Liu, Y.; Kang, Z.; Xiao, D.; Gao, C.; Xu, P.; Ma, C. 2,3-Butanediol catabolism in *Pseudomonas aeruginosa* PAO1. *Environ. Microbiol.* **2018**, *20*, 3927–3940. [\[CrossRef\]](#) [\[PubMed\]](#)
82. Hassett, D.J.; Howell, M.L.; Sokol, P.A.; Vasil, M.L.; Dean, G.E. Fumarase C activity is elevated in response to iron deprivation and in mucoid, alginate-producing *Pseudomonas aeruginosa*: Cloning and characterization of fumC and purification of native fumC. *J. Bacteriol.* **1997**, *179*, 1442–1451. [\[CrossRef\]](#) [\[PubMed\]](#)
83. Wargo, M.J.; Szwergold, B.S.; Hogan, D.A. Identification of two gene clusters and a transcriptional regulator required for *Pseudomonas aeruginosa* glycine betaine catabolism. *J. Bacteriol.* **2008**, *190*, 2690–2699. [\[CrossRef\]](#) [\[PubMed\]](#)
84. Hampel, K.J.; LaBauve, A.E.; Meadows, J.A.; Fitzsimmons, L.F.; Nock, A.M.; Wargo, M.J. Characterization of the GbdR regulon in *Pseudomonas aeruginosa*. *J. Bacteriol.* **2014**, *196*, 7–15. [\[CrossRef\]](#)
85. Fitzsimmons, L.F.; Hampel, K.J.; Wargo, M.J. Cellular choline and glycine betaine pools impact osmoprotection and phospholipase C production in *Pseudomonas aeruginosa*. *J. Bacteriol.* **2012**, *194*, 4718–4726. [\[CrossRef\]](#)
86. Willsey, G.G.; Wargo, M.J. Sarcosine Catabolism in *Pseudomonas aeruginosa* Is Transcriptionally Regulated by SouR. *J. Bacteriol.* **2016**, *198*, 301–310. [\[CrossRef\]](#)
87. Arai, H. Regulation and Function of Versatile Aerobic and Anaerobic Respiratory Metabolism in *Pseudomonas aeruginosa*. *Front. Microbiol.* **2011**, *2*, 103. [\[CrossRef\]](#)
88. Alvarez-Ortega, C.; Harwood, C.S. Responses of *Pseudomonas aeruginosa* to low oxygen indicate that growth in the cystic fibrosis lung is by aerobic respiration. *Mol. Microbiol.* **2007**, *65*, 153–165. [\[CrossRef\]](#)
89. Sabra, W.; Kim, E.J.; Zeng, A.P. Physiological responses of *Pseudomonas aeruginosa* PAO1 to oxidative stress in controlled microaerobic and aerobic cultures. *Microbiology* **2002**, *148*, 3195–3202. [\[CrossRef\]](#)
90. Pedraz, L.; Blanco-Cabra, N.; Torrents, E. Gradual adaptation of facultative anaerobic pathogens to microaerobic and anaerobic conditions. *FASEB J.* **2020**, *34*, 2912–2928. [\[CrossRef\]](#)
91. Schreiber, K.; Krieger, R.; Benkert, B.; Eschbach, M.; Arai, H.; Schobert, M.; Jahn, D. The anaerobic regulatory network required for *Pseudomonas aeruginosa* nitrate respiration. *J. Bacteriol.* **2007**, *189*, 4310–4314. [\[CrossRef\]](#) [\[PubMed\]](#)
92. Yoon, S.S.; Karabulut, A.C.; Lipscomb, J.D.; Hennigan, R.F.; Lyman, S.V.; Groce, S.L.; Herr, A.B.; Howell, M.L.; Kiley, P.J.; Schurr, M.J.; et al. Two-pronged survival strategy for the major cystic fibrosis pathogen, *Pseudomonas aeruginosa*, lacking the capacity to degrade nitric oxide during anaerobic respiration. *EMBO J.* **2007**, *26*, 3662–3672. [\[CrossRef\]](#) [\[PubMed\]](#)

93. Crack, J.C.; Green, J.; Thomson, A.J.; Le Brun, N.E. Iron-sulfur clusters as biological sensors: The chemistry of reactions with molecular oxygen and nitric oxide. *Acc. Chem. Res.* **2014**, *47*, 3196–3205. [[CrossRef](#)] [[PubMed](#)]
94. Achebach, S.; Selmer, T.; Udden, G. Properties and significance of apoFNR as a second form of air-inactivated [4Fe-4S]FNR of *Escherichia coli*. *FEBS J.* **2005**, *272*, 4260–4269. [[CrossRef](#)]
95. Dibden, D.P.; Green, J. In vivo cycling of the *Escherichia coli* transcription factor FNR between active and inactive states. *Microbiology* **2005**, *151*, 4063–4070. [[CrossRef](#)]
96. Trunk, K.; Benkert, B.; Quack, N.; Munch, R.; Scheer, M.; Garbe, J.; Jansch, L.; Trost, M.; Wehland, J.; Buer, J.; et al. Anaerobic adaptation in *Pseudomonas aeruginosa*: Definition of the Anr and Dnr regulons. *Environ. Microbiol.* **2010**, *12*, 1719–1733. [[CrossRef](#)]
97. Clay, M.E.; Hammond, J.H.; Zhong, F.; Chen, X.; Kowalski, C.H.; Lee, A.J.; Porter, M.S.; Hampton, T.H.; Greene, C.S.; Pletneva, E.V.; et al. *Pseudomonas aeruginosa* lasR mutant fitness in microoxia is supported by an Anr-regulated oxygen-binding hemerythrin. *Proc. Natl. Acad. Sci. USA* **2020**, *117*, 3167–3173. [[CrossRef](#)]
98. Fulop, V.; Ridout, C.J.; Greenwood, C.; Hajdu, J. Crystal structure of the di-haem cytochrome c peroxidase from *Pseudomonas aeruginosa*. *Structure* **1995**, *3*, 1225–1233. [[CrossRef](#)]
99. Chung, I.Y.; Kim, B.O.; Jang, H.J.; Cho, Y.H. Dual promoters of the major catalase (KatA) govern distinct survival strategies of *Pseudomonas aeruginosa*. *Sci. Rep.* **2016**, *6*, 31185. [[CrossRef](#)]
100. Lin, Y.C.; Sekedat, M.D.; Cornell, W.C.; Silva, G.M.; Okegbe, C.; Price-Whelan, A.; Vogel, C.; Dietrich, L.E.P. Phenazines Regulate Nap-Dependent Denitrification in *Pseudomonas aeruginosa* Biofilms. *J. Bacteriol.* **2018**, *200*. [[CrossRef](#)]
101. Kertesz, M.A. Riding the sulfur cycle—metabolism of sulfonates and sulfate esters in gram-negative bacteria. *FEMS Microbiol. Rev.* **2000**, *24*, 135–175. [[CrossRef](#)] [[PubMed](#)]
102. Guédon, E.; Martin-Verstraete, I. Cysteine Metabolism and Its Regulation in Bacteria. In *Amino Acid Biosynthesis~Pathways, Regulation and Metabolic Engineering. Microbiology Monographs*; Wendisch, V.F., Ed.; Springer: Berlin/Heidelberg, Germany, 2006; Volume 5.
103. Tralau, T.; Vuilleumier, S.; Thibault, C.; Campbell, B.J.; Hart, C.A.; Kertesz, M.A. Transcriptomic analysis of the sulfate starvation response of *Pseudomonas aeruginosa*. *J. Bacteriol.* **2007**, *189*, 6743–6750. [[CrossRef](#)] [[PubMed](#)]
104. Aguilar-Barajas, E.; Diaz-Perez, C.; Ramirez-Diaz, M.I.; Riveros-Rosas, H.; Cervantes, C. Bacterial transport of sulfate, molybdate, and related oxyanions. *Biometals* **2011**, *24*, 687–707. [[CrossRef](#)] [[PubMed](#)]
105. Hummerjohann, J.; Kuttel, E.; Quadroni, M.; Ragaller, J.; Leisinger, T.; Kertesz, M.A. Regulation of the sulfate starvation response in *Pseudomonas aeruginosa*: Role of cysteine biosynthetic intermediates. *Microbiology* **1998**, *144 Pt 5*, 1375–1386. [[CrossRef](#)]
106. Li, K.; Xin, Y.; Xuan, G.; Zhao, R.; Liu, H.; Xia, Y.; Xun, L. *Escherichia coli* Uses Separate Enzymes to Produce H₂S and Reactive Sulfane Sulfur From L-cysteine. *Front. Microbiol.* **2019**, *10*, 298. [[CrossRef](#)]
107. Shen, J.; Peng, H.; Zhang, Y.; Trinidad, J.C.; Giedroc, D.P. *Staphylococcus aureus* sqr Encodes a Type II Sulfide: Quinone Oxidoreductase and Impacts Reactive Sulfur Speciation in Cells. *Biochemistry* **2016**, *55*, 6524–6534. [[CrossRef](#)]
108. Jarrett, J.T. Biotin synthase: A role for iron-sulfur clusters in the radical-mediated generation of carbon-sulfur bonds. In *Iron-Sulfur Clusters in Chemistry and Biology*; Rouault, T.A., Ed.; De Gruyter: Berlin, Germany, 2014.
109. Mihara, H.; Esaki, N. Bacterial cysteine desulfurases: Their function and mechanisms. *Appl. Microbiol. Biotechnol.* **2002**, *60*, 12–23. [[CrossRef](#)]
110. Atta, M.; Arragain, S.; Fontecave, M.; Mulliez, E.; Hunt, J.F.; Luff, J.D.; Forouhar, F. The methylthiolation reaction mediated by the Radical-SAM enzymes. *Biochim. Biophys. Acta* **2012**, *1824*, 1223–1230. [[CrossRef](#)]
111. Nelson, C.E.; Huang, W.; Brewer, L.K.; Nguyen, A.T.; Kane, M.A.; Wilks, A.; Oglesby-Sherrouse, A.G. Proteomic Analysis of the *Pseudomonas aeruginosa* Iron Starvation Response Reveals PrrF Small Regulatory RNA-Dependent Iron Regulation of Twitching Motility, Amino Acid Metabolism, and Zinc Homeostasis Proteins. *J. Bacteriol.* **2019**, *201*. [[CrossRef](#)]
112. Yue, X.; Guidry, J.J. Differential Protein Expression Profiles of Bronchoalveolar Lavage Fluid Following Lipopolysaccharide-Induced Direct and Indirect Lung Injury in Mice. *Int. J. Mol. Sci.* **2019**, *20*, 401. [[CrossRef](#)]
113. Kanehisa, M.; Sato, Y. KEGG Mapper for inferring cellular functions from protein sequences. *Protein Sci.* **2020**, *29*, 28–35. [[CrossRef](#)] [[PubMed](#)]
114. Ulrich, E.L.; Akutsu, H.; Doreleijers, J.F.; Harano, Y.; Ioannidis, Y.E.; Lin, J.; Livny, M.; Mading, S.; Maziuk, D.; Miller, Z.; et al. BioMagResBank. *Nucleic Acids Res.* **2008**, *36*, D402–D408. [[CrossRef](#)] [[PubMed](#)]

115. Wishart, D.S.; Feunang, Y.D.; Marcu, A.; Guo, A.C.; Liang, K.; Vazquez-Fresno, R.; Sajed, T.; Johnson, D.; Li, C.; Karu, N.; et al. HMDB 4.0: The human metabolome database for 2018. *Nucleic Acids Res.* **2018**, *46*, D608–D617. [[CrossRef](#)] [[PubMed](#)]

Publisher’s Note: MDPI stays neutral with regard to jurisdictional claims in published maps and institutional affiliations.



© 2020 by the authors. Licensee MDPI, Basel, Switzerland. This article is an open access article distributed under the terms and conditions of the Creative Commons Attribution (CC BY) license (<http://creativecommons.org/licenses/by/4.0/>).